

Toward spatial impedance estimation for robotic systems

D. (Damiano) Graziosi

MSc Report

Committee:

Dr.ir. D. Dresscher
Dr.ir. N. van der Stap
Dr.ir. P.C. Breedveld
Dr.ir. R.G.K.M. Aarts

September 2018

039RAM2018
Robotics and Mechatronics
EE-Math-CS
University of Twente
P.O. Box 217
7500 AE Enschede
The Netherlands

TNO

UNIVERSITY OF TWENTE.

MIRA CTIT
BIOMEDICAL TECHNOLOGY
AND TECHNICAL MEDICINE

Preface

This thesis concludes my two-year path within the Robotics & Mechatronics department at the University of Twente, leading me to the completion of the MSc program in Systems and Control. Special thanksgivings are due to my university supervisor dr. ir. Douwe Dresscher for his guide, and to the company supervisor dr. ir. Nanda van der Stap for hosting me at TNO and making this collaboration possible.

During this time, I have had the good fortune of encountering people I will always remember, who made this experience truly priceless.

I wholeheartedly thank the university staff for giving me the opportunity to develop myself, and my friends all for making me laugh during those frequent grumpy days.

Finally, I can not refrain from expressing my inmost gratitude to my parents and my brother Matteo for their unconditional presence.

Damiano Graziosi
Enschede, the 21st of September 2018

Summary

In present days, performing complex tasks from a remote site through the use of intermediate mechatronic systems is not an illusion anymore (one can think of the Da Vinci surgical system, for example). That is why telepresence and telemanipulation are topics of research and development within the i-Botics Joint Innovation Center - a collaboration between the University of Twente and TNO. Combining the cognitive ability of the human operator with the robotic capabilities at a distance is the main objective of this cooperation.

Robots never get tired, neither bored nor injured. However, they are still far away from understanding a situation through the senses human beings have been developing for thousand of hundreds of years of evolution on Earth. Therefore, improving these sensing capabilities would allow them to be used even more in complicated tasks where those human abilities and “situational awareness” are required, avoiding human presence in hazardous scenarios (one can think of EOD or pipe inspection robots).

In a typical teleoperated system, unavoidable latencies in between operator (master) and the end-robot (at the slave site) jeopardise transparency (haptic performance) and endanger stability. However, it is known from previous studies that having available a more accurate model of the remote environment, i.e. where the manipulation takes place, would enhance the overall performance the system. For this purpose, an adaptive impedance law can be implemented on each controller side when force/position measurements are available within the Bilateral Impedance Control architecture.

Within a typical teleoperation scheme, this assignment focused on the remote side where, embracing previous implementations, it aimed to enhance the recognition of the real environment in 3D space. It has been accomplished by means of an on-line estimation of the dynamic properties of the physical surrounding, when a 7 DOF telecontrolled robotic arm interacts with it. Within the same operational scenario and making use of these estimates, the system can be then trained to have available a first rough assessment of those physical properties by the only visual data. Eventually, these attributes can be clustered and associated to the corresponding item in the reconstructed virtual world, so as to end up with a “multisensorial picture” of the reality.

Contents

1	Introduction	1
1.1	Problem context	1
1.2	Problems description	2
1.3	Research goal	5
1.4	Evaluation	6
1.5	Related work	8
1.6	Outline of the report	9
2	Background	10
2.1	Impedance & admittance	10
2.2	Bilateral teleoperation scheme	11
2.3	Haptic rendering architectures	12
2.4	Experimental setup	13
3	Problem analysis	15
3.1	Contact models	15
3.2	Friction models	19
3.3	Estimation	20
4	Design and implementation	26
4.1	Simulations	26
4.2	Experimental phase	26
4.3	Experiment design	28
4.4	Visual identification	33
5	Results	35
5.1	Simulations	35
5.2	Experiments	37
5.3	Visual data	44
6	Conclusions	48
6.1	Introduction	48

6.2 Findings and their implications	48
6.3 Recommendations	50
6.4 Conclusion	50
A Supplementary material	52
A.1 Additional plots	52
A.2 Drawings	60
Bibliography	61

1 Introduction

1.1 Problem context

1.1.1 Telemanipulation

Telemanipulation is considered one of the earliest manifestation of modern robotics (Siciliano and Khatib, 2016); in fact, it can be dated back in the 1940s with the pioneering studies conducted by Goertz (Goertz, 1952, 1954) in which he presented a system to manipulate radioactive material. At the same time, he coined a terminology that is still commonly accepted: *master* site stands for the local environment (LE) in which the human operator makes decisions while *slave* indicates the remote environment (RE), where the telecontrolled robot executes the commanded actions.

In its early days, telemanipulation aimed to separate the brain (i.e. whoever plans the task) from the body (i.e. whatever executes it); on the other hand, the latest trend in robotics tends to reconcile these entities by mean of increasing the decision making capability of the robot itself. As noticeable, other terms are used almost interchangeably to indicate telemanipulation, such as telerobotics and teleoperation. While they all share the prefix *tele*, from the Greek word *τηλε* which means "far off", they put emphasis on different targets: on the object-level manipulation, on the human action of controlling a robot and on the task-level operations, respectively.

However, the commonly accepted goal of these tele-*something* research is to avoid human beings presence within the RE which, in some cases, might put their safety at risk (e.g. nuclear industry), present scaling factors (dimensions or forces, for example) unobtainable using the solely human body capabilities or be extremely costly to reach (e.g. space applications).

Telepresence In telerobotic operations (e.g. for maintenance tasks), the ideal case scenario sees an operator whose senses are realistically provided with simulated information as he/she were into the telemanipulated environment, that is the concept of *ultimate telepresence*. Therefore, based on his/her own timely perceptions, correcting actions are commanded to carry on the task. Besides, supportive technologies might allow to have even a better insight into the tasks in hand, and advanced mechatronics systems would let him/her to perform the job while meeting the demanded specifications. As the current state of affair, this picture is pure utopia; in fact, hurdles stand at both sides of a typical teleoperation scheme, as the one in figure 1.2. For example, the discrete nature of the communication in between the hardware wipes out the concept of "absolutely real time" operations. Moreover, the entire framework is based on the assumption that the environment is immediately recognised, and information from the remote site are continuously -not discretely- reflected to the operator so as to simultaneously stimulate his/her touch, sight, hear, smell and taste senses. Eventually, the more realistic the operator's experience will be, the better the tasks will be executed.

1.1.2 Environment exploration

For the sake of simplicity, based on the extent of the *a priori* knowledge, an operator can face with a:

- totally known RE;
- partially known RE;
- totally unknown RE.

Within each of the above mentioned cases, likewise the tasks to be carried out could be:

- fully determined;
- partially determined;
- totally determined.

Figure 1.1 sketches the transitions that are needed to determine if and how a task can be carried out: the knowledge about the environment and the duty to tackle are the ordinate and abscissa respectively, while the third axis represent the extent of autonomusness of the mechatronic system.

Determining if and how a task can be executed passes through a minimal knowledge of the environment; i.e. a threshold which depends on the application in hand. For example, if a robot has to grab a glass on a table, awareness about the location of the objects within the 3D space are needed, whereas only a partial recognition of the surrounding area is necessary for that job. When this requisite limit is not yet reached, that is an environment still very unknown, then a further exploration for recognition is needed - upward vertical direction into figure 1.1. Besides, artificial intelligence (AI) techniques together with the dexterous manipulative development of the robots, push this path toward the third dimension in figure 1.1. The ideal goal is represented by a total and thorough knowledge of the remote environment to fully determine how to accomplish the desired task. The latter, as already said, would be fully given only when the real world is known for a reasonable extent: i.e. when the threshold band in figure 1.1 is reached.

This concept can be for example applied to the very hot topic of human-robot interaction (HRI), where safety is the primary concern: in fact, robots could not safely and "friendly" interact with humans if the boundary conditions (i.e. the RE) are only blurry known.

1.2 Problems description

Nowadays, the ultimate goal of these master-slave systems is to reflect feedback(s) to the operator in a way that he/she would perceive the environment as if being present at the remote site. From that, the terms virtual reality (VR) will be herein used to indicate the set of conditions which make that possible: e.g. an acoustic, visual, tactile and haptic displays. The latter, in particular, establishes a fully bi-directional interface in which mechanical power flows from the operator to the haptic device and vice versa (*bilateral* systems). The forces fed

1.2.2 Transparency and stability

As a matter of definition, transparency of a telerobotic system is defined as the fidelity by which the human operator perceives the RE and the naturalness by which he/she can perform the task within the slave site (Tzafestas et al., 2008). In any case, pursuing total transparency should not come at the stake of a stable systems; in fact, in (Hannaford, 1989b), the author proved that it exist a trade-off in between stability and performance, measured in this case by the grade of transparency. Later on, in (Franken et al., 2009, 2011), the authors proposed a two-layers control architecture to fill the gap in between transparency and passivity by addressing these two properties independently.

1.2.3 Time delay

The communication channel in between the master and the slave allows the data transfer throughout the teleoperation system - defined "barrier" in figure 1.2. Together with foreseeable digital discretization, this information exchange link suffers from unpredictable latencies and low-bandwidth (LF) communications; these questions are even more exacerbated by the supposedly extreme conditions of the operational scenario (one can think to underwater operations, for example). These hurdles make often unpractical to use a direct control in between LE and RE to reflect the interaction forces to the operator, viz. singly position/force controller.

In order to remove this dependency on the time delay introduced by the communication channel, a commonly used alternative is to make the operator interact with an fictitious reproduction (either partially or made completely up) of the remote environment, herein meant as a graphical virtual environment (VE). This situation sees an operator who telemanipulates objects inside a VE which is timely updated -communication channel allowing- upon measured and processed signals from the remote environment. Therefore, through a physics engine (section 2.3), the desired sensory stimuli are transmitted to the user to convey information about a virtual haptic object.

This so built virtual world, constructed upon these new knowledge, would remove the communication latency and data loss dependency which practically always occur in direct telerobotic operations. Potentially, this VE can be seen as a time-delay free middle ground, in which the operator works safely, effectively, inexpensively and rapidly trains specific skills..

1.2.4 Actuator and sensory capability

Ones of the biggest challenges telerobotic faces are the timing and resolution constrains imposed by the human body physiology. In fact, the term haptic comes from the Greek word *απτεισθαι* (haptesthai) which means "to touch", specifically via kinesthetic (force/position) and cutaneous (tactile) receptors, controlled by the human nervous system. This biological mechanism works at the average frequency of 1 *kHz* – 10 *kHz* and very small sensible displacements 2 – 4 μm (Shimoga, 1993); this fact is even more important when dealing with stiff material where incredibly high bandwidth (up to 20 *kHz*) are needed to achieve stability (Siciliano and Khatib, 2016). In practice, these fidelity and frequency range can

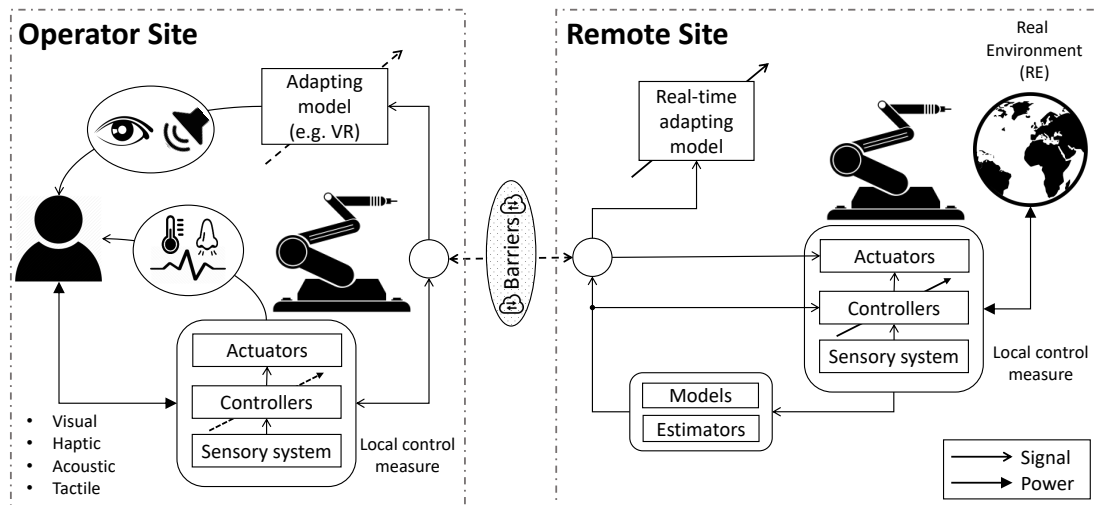


Figure 1.2: General structure of a teleoperated system.

not be achieved within an open loop operational mode, and this is another reason why haptic rendering¹ is driving much of today's haptic virtual environment research, this project included.

1.3 Research goal

Generally speaking, the final goal of every controlled system is to have a complementary sensitivity function $T(s) = \frac{Y(s)}{U(s)} = 1$ within a specific range of frequency. Therefore, promptly knowing the plant behaviour (i.e. its state vector) would allow to generate specific correcting actions to seek that result. In fact, while predictable deviations from the ideal behaviour could be compensated by applying feed-forward, more complex and unforeseen dynamics can only be dealt inside a feedback loop -within the robustness range. In practice, the sensory capability of mechatronic systems could be limited and the state vector x only partially known: that is why estimation theory comes to help engineers to design adaptive controller (e.g. MRAS or STR).

1.3.1 i-Botics

Within *i-Botics*, the long-term goal is to automate the environment recognition, along with building a virtual environment in order allow users to perform finer tasks in hazardous environment by means of telerobotic systems. The ultimate goal is to combine visual

¹I.e. determining interaction forces with virtual objects when the operator's motion is measured (for impedance haptic devices)

recognition and dynamic identification of the environment to autonomously accomplish otherwise dangerous operations. An example could be inspection/rescue routine tasks; at the same time, the human operator would supervise the mission and fine tunes the details, where needed. A major advantage of this telerobotics approach is that it optimally benefits from combining the cognitive ability of the human operator with the robotic capabilities at a distance.

1.3.2 Research questions

Referring to section 1.2, this research investigates possible relives to the latency issue which, in turn, would result in improved performance, the transparency in particular. Specifically, plenty of studies advocated that an upfront (ideally) or online knowledge about the nature of the real environment would lead to such an enhanced telepresence. However, the validation of this claims come from simplistic case studies in which ad-hoc experimental setups have been employed, and the environment has the dimension of a point. Based on these premises, the following research questions have be formulated:

How can a punctual estimation of the dynamic properties of the environment be extended into the 3D space, while employing a realistic multi-DOF robotic manipulator?

By means of solely visual data, would it be possible to forecast the same properties?

When it comes to Robotics, one can distinguish constrained from unconstrained tasks: i.e. when the robot physically interacts with the real surrounding (grinding operations, for example) and when it does not (e.g. visual inspection), respectively.

This project focuses chiefly on the environment identification by means of constrained interactions. Besides, it aims to lay the foundations for an RE recognition through the solely visual data (unconstrained task) so as to push the system autonomusness a step forward. As the result from a parallel research within i-Botics ([Hoeba et al., 2018](#)), when using a rgb-d sensor camera, a virtual 3D representation of the environment is built up and made available for visual feedback to the operator.

Other works focused on the friction coefficient(s) determination, likewise essential for the tactile perception during manipulative tasks. Based on that, this project aims to simultaneously estimate the generalised impedance Z_e , namely stiffness K and damping B , together with the friction coefficient(s) of the real environment in order endow the VR geometrical description with meaningful physical features.

1.4 Evaluation

Due to the lack of infinite sensory capability every mechatronic device is prone to, it is not always possible to fully measure the state of the system; for instance, based on the available measured data, estimation techniques have to be applied. Hence, a physical interaction in between end-effector of the slave robot and environment, together with a contact model for this phenomenon are superimposed; from that, the physical parameters of the model itself

will be recursively estimated in real time.

A set up consisting of a cube-shaped material will serve for the purpose of resembling a realistic case situation. This block has been purposely made such that sub-areas with different characteristics can be visually distinguished. The same will be intentionally poked by the end effector of a Kuka LWR robotic arm (section 2.4).

Since the main objective of this research hovers around the slave side of a typical bilateral teleoperation scheme - as in figure 1.3 - the operator contribution together with the related haptic feedback capabilities will not be addressed anymore. For instance, the supposedly arbitrary commanded motion of the operator is replaced by a generated reference path (GRP) the robot follows to approach and to interact with the real surrounding.

Thereafter, the above mentioned physical properties will be recursively estimated² from the knowledge of the reference kinematics, the measured forces and mathematical models that describe the contact phenomena.

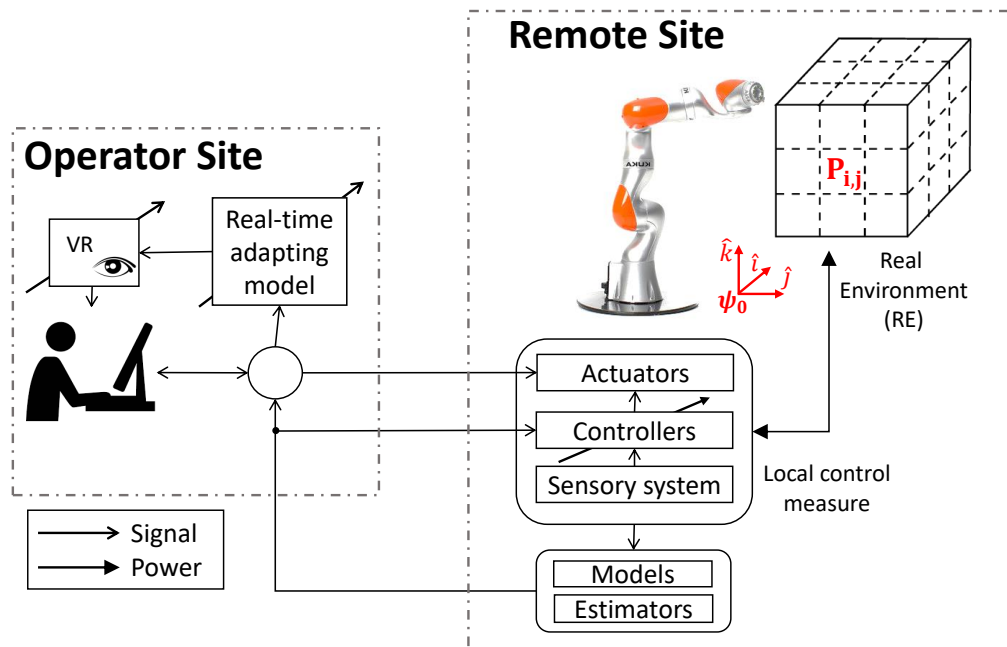


Figure 1.3: The main focus of this work will be on the slave side.

Bottom line

Eventually, this work aims to:

- a fitted 3D mapping $M_p = [B_{i,j}, B_{i,j}, \mu_{i,j}] \forall \Phi_0 P_{i,j}$ of the dynamic properties, estimated by means of physical interaction robot/environment;

²Under the quasi-static assumption, viz. non accelerating systems

- a mapping $M_v \in \mathbb{R}^n \forall {}^0P_{i,j}$, which defines the point-wise (or averaged) visual distinguishing features $\forall {}^0P_{i,j}$ of the physical surrounding.

For the sake of simplicity, the geometry of the real environment is assumed to be known in advance; in particular, a flat surface has been selected.

Ultimately, all these pieces of information lead to outline an intuitive *modus operandi* which can help to push the environment recognition matter a bit more toward the AI trend. In fact, all these data sources can be overlapped in order to find characteristic patterns inside the visual data such that those physical properties can be foreseen in alike circumstances. This approach aims to avoid likely destructive physical interactions, especially when dealing with delicate environments (e.g. biological tissues).

1.5 Related work

Within this area of study, it is right and proper to mention (Hogan, 1985), in which the author coined the impedance control concept; it is considered the baseline upon which many modern frameworks in telerobotics are built upon.

In (Ueberle et al., 2009; Sheridan, 1989, 1993; Hokayem and Spong, 2006), extensive surveys about teleoperated systems turn out to give an overview of the current state of affair about the topic.

It all comes to the measure of performance of the system, namely stability and transparency. The former concept has been the main topic in (Colgate and Brown, 1994; Hannaford, 1989b) - seen in its classical fashion - while Franken et al. presented a novel passivity theory in (Franken et al., 2009, 2011) to deal with energy bounded systems. The concepts of bilateral teleoperation and impedance reflection (IR) method have been introduced in (Hannaford, 1989a; Hannaford and Fiorini, 1988), relevant references for many of following researches into this area of study.

From that, adaptive impedance control architectures have been studied and implemented in (Velanas and Tzafestas, 2010; Tzafestas et al., 2008; Abdossalami and Sirouspour, 2008; Love and Book, 2004; Na and Vu, 2012; Misra and Okamura, 2006), among others.

Besides, the estimation of the physical properties of the environment has been carried out in (Biagiotti and Melchiorri, 2007; Yamamoto et al., 2008; Diolaiti et al., 2005; Haddadi and Hashtrudi-Zaad, 2008, 2012).

Virtual environment, in the form of augmented reality (AR) or virtual reality (VR) are by now important topics in Robotics and its research is fuelled by different industries; in (Jeon and Choi, 2009, 2010), the authors lay down definitions and applications.

To achieve perfect fulfilment of task in teleoperation mode, viz. total transparency while ensuring stability, haptic devices should reflect to the user the same object properties as the ones perceptible within the *exploratory procedures* (EPs) classification as defined by the authors in (Lederman and Klatzky, 1987; Klatzky et al., 1985; Lederman and Klatzky, 1990).

Although the current state of the art does not permit all of these EPs at the same time, such a classification helps to break down the problem and to address them singularly. Among the other variables, the vigour with which the operator holds the haptic device has important consequences to the overall performance of the system (Velanas and Tzafestas, 2010). For instance, a model adaptive reference control (MRAC) to compensate for dynamics forces caused by the hand was proposed in (Na and Vu, 2012).

When it comes to contact models, in (Hunt and Crossley, 1975) a neat and clear treatise highlights the superiority of such a novel description over other used model. Besides, Gilardi et al. made an insightful survey in contact dynamics modelling in (Gilardi and Sharf, 2002), comparing the Hunt-Crossley model with others.

How to face with friction and model it in telecontrolled systems is the core of (Bicchi et al., 1993), whereas in (Siciliano and Khatib, 2016) a later survey overarches upon its historical background and the modern approaches to deal with it.

1.6 Outline of the report

Following this introduction, chapter 2 contains theories and information not strictly needed for the practised readers, although interesting and worthy to be mentioned. A more theoretical analysis will be presented in chapter 3. Thereupon, simulations and experiments reported in chapter 4 aim to give a more realistic connotation to those speculative foundations. The outcome will be critically analysed within chapter 5, while conclusion and recommendations will close the report.

2 Background

2.1 Impedance & admittance

2.1.1 Device type

In (Hogan, 1985), the author discerns a device type classification from causality considerations: for instance, in any physical system, power instantaneously flows from one "point" to the other (e.g. robot/environment interaction) if a state variable varies. As the power is the product of two conjugate variables, namely effort and flow, any system can impose a force or a displacement (or velocity) separately, keeping the manipulator example. system along each DOF, and (Ott et al., 2010), for example. From that, Hogan distinguishes admittance and impedance type for every physical system: the former accept effort and release flow whereas the latter behaves in a dual way. Moreover, to ensure physical compatibility, in any dynamic interaction there has to be an impedance and an admittance system. And when it comes to manipulative tasks, the environment contains inertia and/or kinematic constraints, i.e. admittance type systems as seen from the manipulator point of view; hence, the manipulator behaves as an impedance. In (Ott et al., 2010), the authors outlined typical pros and cons for the two types.

2.1.2 Impedance controller

In a very trivial fashion, as already mentioned, achieving full transparency would mean having a slave robots which perfectly and timely follows the master position, that is $F_m = -F_s$. To this end, a possible controller design is the one presented in (Stramigioli, 1998). It calculates the correcting torques by means of a wrench $W^{0,ee}$ into the reference frame, which is proportional to the difference in between the set-point position and the end-effector location as there was a mechanical spring in between the master and the slave devices. Herein, the assumption is that both of them are impedance type. Referring to figure 2.1, it obeys to the relation:

$$F_s = K_v (x_m - x_s) \quad (2.1)$$

where F_m , F_u and F_s are the master, user and slave controller output forces, respectively. In (Nijof, 2018), an extension of this concept with an added damping effect is described (viz. joint damping).

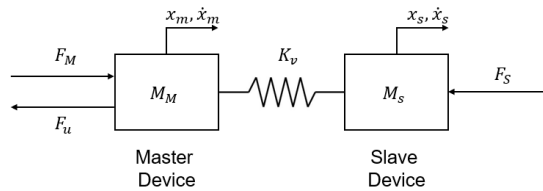


Figure 2.1: Impedance controller schematic.

2.2 Bilateral teleoperation scheme

Back in 1989, Hannaford (Hannaford, 1989a) introduced a two-ports hybrid model for teleoperated systems. Human operator and environment are fully described analysing the power conjugated effort $e_{h/e}$ (forces) and flow $f_{h/e}$ (velocities) variables (Broenink, 1999). By choosing the two dependent/independent variables, one is *de facto* imposing the causality of the constitutive equations which describe the system. For example, when the force at position are available at the slave side, the two-port hybrid formulation becomes¹:

$$\begin{bmatrix} e_h \\ f_h \end{bmatrix} = \begin{bmatrix} h_{11} & h_{12} \\ h_{21} & h_{22} \end{bmatrix} \begin{bmatrix} f_e \\ e_e \end{bmatrix} \quad (2.2)$$

However, when interaction occurs, the position of the slave $q_e = \frac{df_e}{dt}$ can be correlated to the force F_e via the multivariable impedance function Z_e (Lawrence, 1992), which, in principle, can have an arbitrary form alike $F_e = Z_e(q_e)$. Then, for the sake of simplicity, the linear case is considered such that:

$$F_e = Z_e q_e \quad (2.3)$$

Therefore, the h_{ij} values into the system 2.2 can be interpreted as:

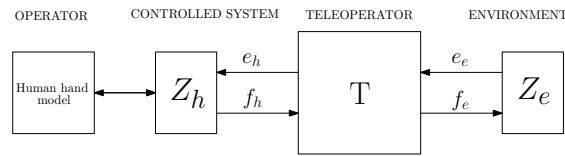


Figure 2.2: Two-ports model of a teleoperated system.

$$H_{hybrid} = \begin{bmatrix} h_{11} & h_{12} \\ h_{21} & h_{22} \end{bmatrix} = \begin{bmatrix} Z_e & K_F \\ K_v & \frac{1}{Z_h} \end{bmatrix} \quad (2.4)$$

where K_F and K_v are force and scaling factors respectively. Taking advantage of this notation, one can rephrase the ideal transparency concept in terms of:

$$\begin{aligned} e_h &= e_e \\ f_h &= f_e \end{aligned} \quad (2.5)$$

It happens *iff* the impedance transmitted to the operator Z_h is equal to the one showed by the environment, that is:

$$Z_h = Z_e \quad (2.6)$$

It comes from here this concept the impedance reflection (IR) definition. Solving the system 2.2 for e_h and f_h , and using equation 2.6, then:

$$e_h = \underbrace{(h_{11} - h_{12}Z_e)(h_{21} - h_{22}Z_e)^{-1}}_{Z_h} f_h \quad (2.7)$$

¹Everything is described within the frequency domain (Laplace transform) and the complex operator "s" is dropped for clarity.

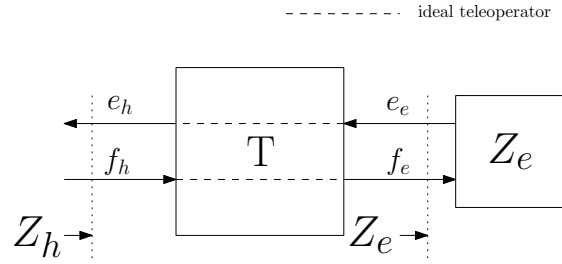


Figure 2.3: Transmitted impedance.

This relations claims that perfect transparency occurs *iff* $h_{11} = h_{22} = 0 \wedge h_{21} = -h_{12}$, confirming that the h matrix for an ideal teleoperator looks like:

$$h_{ideal} = \begin{bmatrix} 0 & 1 \\ -1 & 0 \end{bmatrix} \quad (2.8)$$

The same reasoning can be applied at the slave side if the "human hand impedance" Z_h were considered. Eventually, in (Hannaford, 1989a), the "bilateral impedance control architecture" has been proposed: both sides of the teleoperation scheme are equipped with a local control law which enforces estimated impedance and force of the other side. It is worthy to mention that such a two-port model, is a linear system, hence valid only around equilibrium points; for example, non-linear delaying terms e^{-st} should be addressed differently (Hannaford, 1989b).

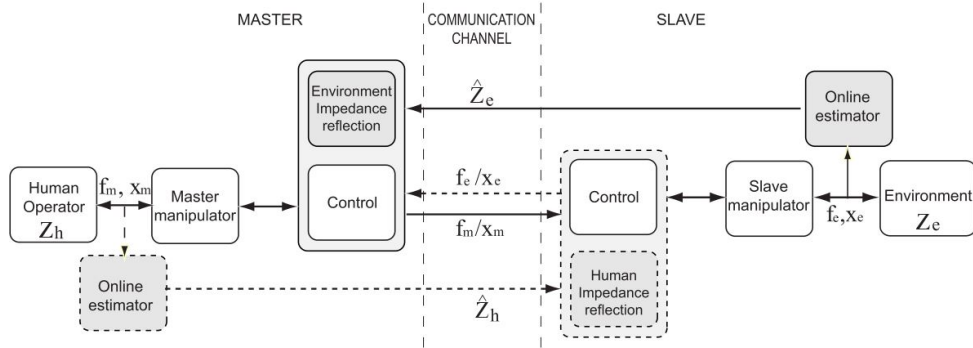


Figure 2.4: Conceptual scheme of the IR in teleoperation.

2.3 Haptic rendering architectures

Haptic rendering algorithms evaluate the interaction forces between the haptic interface representation inside the virtual environment and the virtual objects inside it (Salisbury et al., 2004). Figure 2.5 exemplifies this algorithm: S stands for the contact, X is the position, F_d the interaction force and F_r the rendered one.

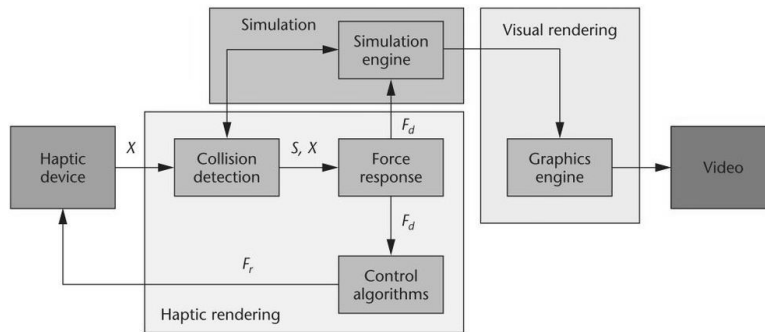


Figure 2.5: Haptic rendering scheme.

2.4 Experimental setup

2.4.1 Hardware

KUKA LWR

Within this investigation, a 7 DOF serial robotic arm KUKA LWR4+ has been employed, as schematically reported in figure 2.6. An internal robot controller (KRC) is connected via UDP to an external computer, and it provides features to compensate for friction and gravity. For instance, through the latter, a set-point could be commanded to the internal impedance (or position) controller, or joint torques as resulting from an external controller.

Due to time constraints, the same implementation as in (Nijof, 2018) has been considered:

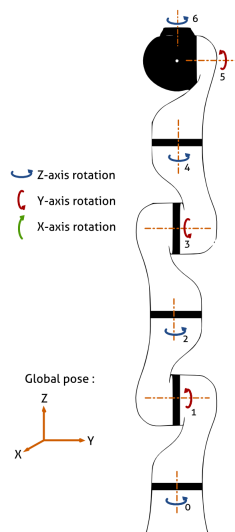


Figure 2.6: KUKA LWR joints.

for instance, the widely used C++ library FRI² allowed to command position setpoints, while running an external impedance controller with a $K_c = 5200$.

²Source: [website](#).

End effector

A blunted end-effector has been purposely designed in order to let the robot interact with the surrounding environment, in such a way to allow smooth poking and surface following (i.e. sliding) motions. Figure 2.7 show the two used tools, whereas the second (rendering 2.7b turn out to be a better design for the purpose: that was because of its stocky shape. In appendix A.2 its he mechanical design is attached.

In between the robotic arm and these tool, a force-torque sensor (ATI MINI40-E³) has

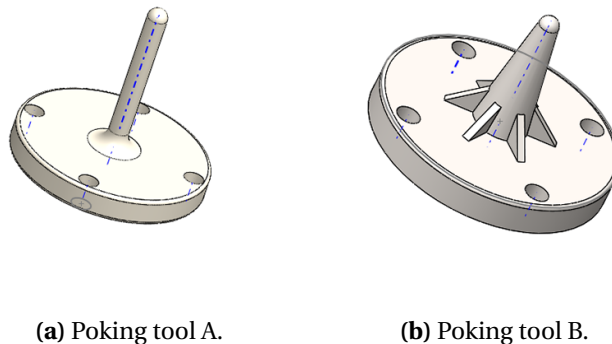


Figure 2.7: Poking tools.

been mounted in order to measure the extent of the dynamic interaction with the real environment.

2.4.2 Software interface

In a modular fashion, commanded set-points, controlled output torques and measured forces/torques are monitored within a ROS⁴ environment. For instance, the commanded set point, the FRI interface, the impedance controller and the force sensor correspond to different *nodes*. In turn, they exchange *messages* through *topics* using the *publishing* and *subscribing* structure, so as to synchronise the *messages* and embed all the modules within a single environment.

³Source: [website](#).

⁴Source: [website](#).

3 Problem analysis

Looking at a typical teleoperation scheme, from the control standpoint, it is well known that a solely force or position control do not suffice for constrained tasks (Erickson et al., 2003); that is the main reason why the impedance control strategy (in its general accepted meaning) proposed by Hogan (Hogan, 1985) is so widely applied. In fact, it aims to adjust both position and force at the same time, when a dynamic relation in between them is superimposed within a single control law (section 2.1). In the most general case it is expressed in a matrix form, so as to address the contribution of each Cartesian variable with respect each other; however, under the simplifying assumption of uncoupled relations, the study can be circumscribed to a single relation.

It has been shown in (Love and Book, 1995) and (Seraji et al., 1996), among others, that when the mechanical properties of the RE are known, the teleoperated system performs better. Knowledge of the environment can be used to optimise control, and having reliable estimates for stiffness and damping coefficients of the physical surrounding, would allow the implementation of more advanced control schemes (Love and Book, 1995). It turns out to better track the reference force and to improve the stability margins of the impedance controllers: i.e. transparency and stability performance would enhance.

With the aim of implementing the IR approach (section 2.2) within further investigations, the goal here is to recursively estimate the impedance of the environment - Z_e , namely stiffness and damping- so as to be used, for example, into the local master controller or to build up a more realistic VR world.

The first step toward the implementation of an online impedance estimation of objects interacting with a robotic device is the choice of a suitable contact models (Erickson et al., 2003).

3.1 Contact models

This section will briefly recall some physical models to describe the interaction in between two bodies, where the first is rigid (slave's end-effector), the second visco-elastic (the real environment). Generally speaking, a model is the first guess scientists use to describe and predict the behaviour of the real world; then, within an iterative and correcting cycle, an experimental validation phase would confirm - or not - its suitability.

3.1.1 Assumptions

In some previous researches (Love and Book, 1995; Hashtrudi-Zaad and Salcudean, 1996) the inertia of the poked body has been estimated too. However, a rather typical assumption in telemanipulation is to consider the teleoperated system to behave through a sequence of equilibrium states. It follows that the sum of all the forces acting upon the body is null. This *quasi-static* assumption describes a "slow" evolution of the system and it allows to neglect the inertial effects.

Moreover, at a microscopic scale, every physical interaction is spreaded throughout a finite number of contact points (centroids), whereas the interaction will herein be studied as a very

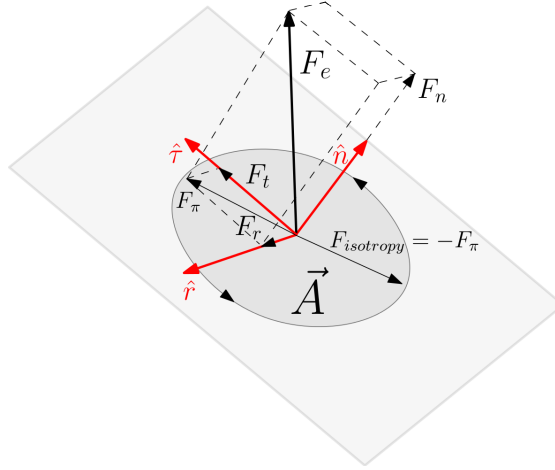


Figure 3.1: Point-wise contact.

point-wise (ideal) contact. The resulting force F_e applied by this point can be decomposed in a tangential, radial and normal components w.r.t. the area A , such that $\|A\|_{\rightarrow 0}$.

That is:

$$\mathbf{F}_e = F_n \mathbf{n} + F_t \boldsymbol{\tau} + F_r \mathbf{r} \quad (3.1)$$

Therefore, assuming persistent contact and isotropic material properties within the plane π spanned by the versors \hat{r} and $\hat{\tau}$, would simplify the problem to consider solely the normal component F_n , acting upon the centroid as sketched in figure 3.1. Eventually,

$$\mathbf{F}_e = F_n \quad (3.2)$$

From now on, the direction of the environmental force F_e will always be the same as \hat{n} , and the vector notation will be replaced by the scalar one.

How this F_e is modelled will be the topic of the following paragraphs: in fact, stiffness, damping and friction coefficients will be illustrated within typical idealised structures.

3.1.2 Linear models

Hooke

The simplest way to model F_n within a virtual environment scenario, for example, is the linear position dependent case. Firstly the point-wise collision is detected, then the haptic interaction point (HIP) -using the same nomenclature as in (Ho et al., 1999)- penetrates the virtual object surface; finally, a commonly used reflected force F_e obeys to the *Hooke's law*:

$$F_e(t) = F_{Hooke}(x) = \begin{cases} 0 & x(t) \leq 0 \\ kx & x(t) > 0 \end{cases} \quad (3.3)$$

where x is the nearest point on the *impedance surface* of the model into the VE and k is the virtual stiffness. It is worth mentioning that the dynamic effect of the impact is not

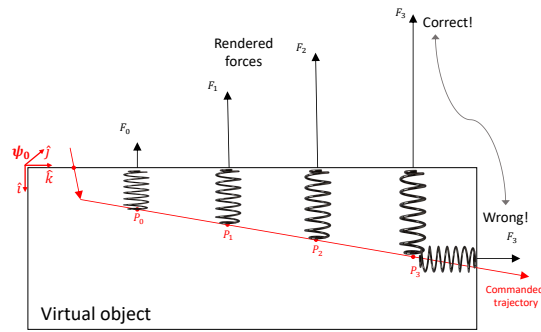


Figure 3.2: Rendered forces.

contemplated within this representation. Although its apparent simplicity, as noticeable from figure 3.2, this model still needs special attentions.

After all, regardless of the adopted model, the resulting rendered forces F , evaluated within the Cartesian space, have to be translated in torques τ applied by the actuators of an hypothetical haptic device. To accomplish that, the transformation

$$\tau(t) = \mathbf{J}^T \mathbf{F}_e(t) \quad (3.4)$$

is used, where \mathbf{J} is the Jacobian matrix of the specific haptic device.

Kelvin-Voight

The pure elastic model can be modified to incorporate other effects, for instance the contribution of an added Newtonian damper. A simple implementation, more commonly known as Kelvin-Voight model, sees a parallel connection in between a spring and a damper; besides, the so called Maxwell and Zener configurations are two other linear ways to ascribe for other physical effects (Biagiotti and Melchiorri, 2007).

$$F_e(t) = F_{KV}(x, \dot{x}) = \begin{cases} 0 & x(t) \leq 0 \\ kx(t) + d\dot{x}(t) & x(t) > 0 \end{cases} \quad (3.5)$$

However, in (Gilardi and Sharf, 2002), the authors summarise the weaknesses the Kelvin-Voight model suffers from:

- as soon as the impact takes place, F_e is discontinuous because of the damping term, and the same happens when the probe loses the contact with the environment. Intuitively, for $x = 0$, both the elastic and viscous components should be null while increasing over time;
- during the rebound phase, as the penetration $x \rightarrow 0$, a negative force holding the bodies together is predicted by this model;
- using the description 3.5, the coefficient of restitution (Marhefka and Orin, 1999) would not depend on impact velocity.

No matter how, for many practical applications, regardless the above mentioned physical inconsistencies, this model is still very simple (great asset) and predicts reasonably the energy dissipation, unconcerned about plastic deformation matters.

The coefficient of restitution e , defined as

$$e = \frac{v_o}{v_i} \quad (3.6)$$

gives an idea about the energy dissipation during the (1 dof) impact in between two rigid bodies. In equation 3.6, v_o and v_i are the relative velocities after and before the contact, respectively. It has been shown (Hunt and Crossley, 1975) that for low v_i , and inside the elastic range of the material, then e can be approximated by:

$$e = 1 - \alpha v_i \quad (3.7)$$

where α is a (low-value) constant, depending on the material and the geometry of the surface in contact.

3.1.3 Non linear models

Hertz

The shortcomings of the Hooke model, can be overcome considering a non-linear elastic force as:

$$F_e(t) = F_{Hertz}(x, n) = \begin{cases} 0 & x(t) \leq 0 \\ k x(t)^n & x(t) > 0 \end{cases} \quad (3.8)$$

where the constant exponent n varies with the material and the shape of the colliding objects. Additional assumptions upon which this model has been derived are (Gilardi and Sharf, 2002):

- the deformation is concentrated in the proximity of A ;
- the elastic wave motion is disregarded;
- the inertia of each of the body is concentrated into their centers of mass.

For completeness, equation 3.8 could be upgraded with additional terms to take into account other phenomena: e.g. hysteresis and plastic deformation.

Hunt-Crossley

Using the previously presented models as building blocks, in order to take into account also the energy dissipation, while keeping coherency with the coefficient of restitution, in (Hunt and Crossley, 1975) the Hunt-Crossley model has been proposed as follows.

$$F_e(t) = F_{HC}(x, \dot{x}, n) = \begin{cases} 0 & x(t) \leq 0 \\ k x(t)^n + d \dot{x}(t)^q x(t)^p & x(t) > 0 \end{cases} \quad (3.9)$$

The "new" parameters are commonly chosen as $p = n$ and $q = 1$.

The main advantage of this model is to have a damping component of the normal force which depends on the extend of the penetration x , *de facto* eliminating those discontinuities at the beginning and at the end of the contact, which are instead present in 3.5.

Using this model, the parameter α in equation 3.7 can be approximated by:

$$\alpha = \frac{2d}{3k} \quad (3.10)$$

therefore solely depending on material properties. In (Diolaiti et al., 2005; Haddadi and Hashtrudi-Zaad, 2008, 2012) it has been proved that this model clearly outperforms the Kelvin-Voight one for softer real environment types (e.g. biological tissues).

From these observations, within this research, the Hunt-Crossley model would be the preferred descriptor of the interaction in between the slave robot and the surrounding physical environment.

3.2 Friction models

Friction is commonly interpreted as the resisting force which arises in between two contacting bodies with non-null relative velocity v . It is a complex and highly non-linear phenomenon for which empiric formulations are often used from case to case. While robotics still lacks of advanced skin-like tactile sensor availability¹, frictional forces are essential to carry out human-like dexterous manipulations; for example, to control the level of slippage. Additionally, moving frictional information within a virtual world model, would extend its overall description and lead to a more realistic experience to the user on the ground that more senses would be stimulated. While friction is often an undesired phenomenon (e.g. in high-precision mechanisms), other times is pursued (i.e. 3D scanners, tyres manufacturing, grasping tasks); however, in both cases, a thorough understanding of this phenomenon would lead to optimised solutions.

In many dexterous manipulations, slippage is seen as an undesirable loss of control, therefore the main concern is about the static friction limits (Bicchi et al., 1993). Therefore, a static friction model, solely dependent on v , will be herein used and validated -or not- within the production phase.

The most common model is built upon the Coulomb friction and a linear viscous damping components, while neglecting adhesion and addressing only (1 dof) compressive forces, such that:

$$\begin{aligned} F_{fric} &= F_{Coulomb} + F_{Kinetic} = \\ &= \mu_{st} F_n \text{sign}(v) + \mu_{kin} v \end{aligned} \quad (3.11)$$

This model can be used to roughly model friction forces for steady-state velocities (Van Geffen, 2009), not close to zero. Specifically, F_n stands for the normal compressive force and the coefficients μ_{st}, μ_{kin} depends on the material properties as well as the geometry of the object in contact. Furthermore, to describe the empirical occurrence of lower friction forces as velocity increases within a bounded region (figure 3.3b), the *Stribeck* effect F_{Str} could be added to equation 3.11. For the sake of thoroughness, more advanced descriptions,

¹Within i-Botics,cite Koen's work

such as the "seven parameters" model, *Dahl* and *LuGre* ones could be considered to take into account other physical details. Hence, looking at figure 3.3a, "far enough" from $v = 0$, one could expect a constant friction force for constant relative velocity v . Due to its simplicity,

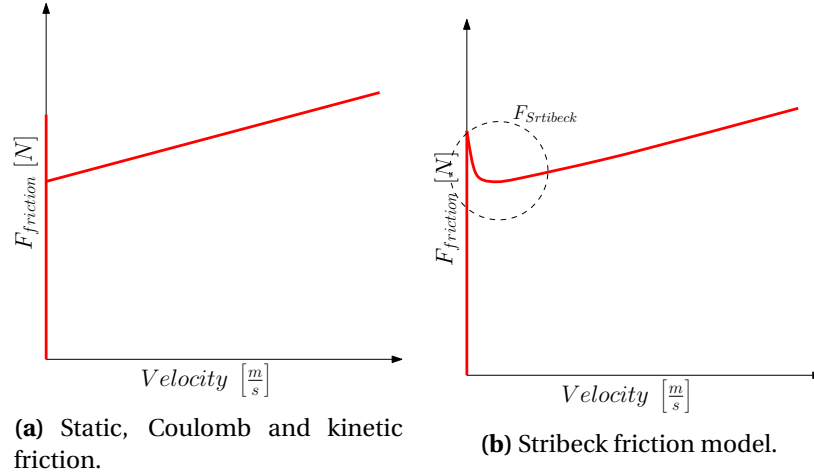


Figure 3.3: Simplistic frictional behaviours.

equation 3.11 was chosen as default for further experiments.

3.3 Estimation

Referring to figure 3.4, and as mentioned in section 1.3, having available trustworthy information about the remote environment would lead to the double benefits of :

1. improving transparency and stability (Diolaiti et al., 2005; Misra and Okamura, 2006; Franken et al., 2011; Hannaford, 1989b; Colgate and Brown, 1994; Hannaford and Fiorini, 1988; Yamamoto et al., 2008; Biagiotti and Melchiorri, 2007);
2. extending the virtual reality paradigm as in figure 3.4 with meaningful physical properties of the real environment. It would yield to a more realistic VE itself and to more reliable haptic reflected forces (haptic rendering); an high-level framework for automatic property identification is presented in (Dupont et al., 1999).

In light of that, considering the comparison study of estimation methods during telemanipulation carried out by Yamamoto et al. in (Yamamoto et al., 2008), together with the works (De Gerssem et al., 2005; Cortesão et al., 2006), a variant of the recursive least square (RLS) has been selected for the following steps of this research. As the name suggests, it can deal with environment models which are linear in the unknown parameter vector (viz. stiffness and damping in this case). Although it does not represent a fully realistic scenario, the previous referred works support the suitability of this procedure for telemanipulation and justify its choice as the selected estimation method.

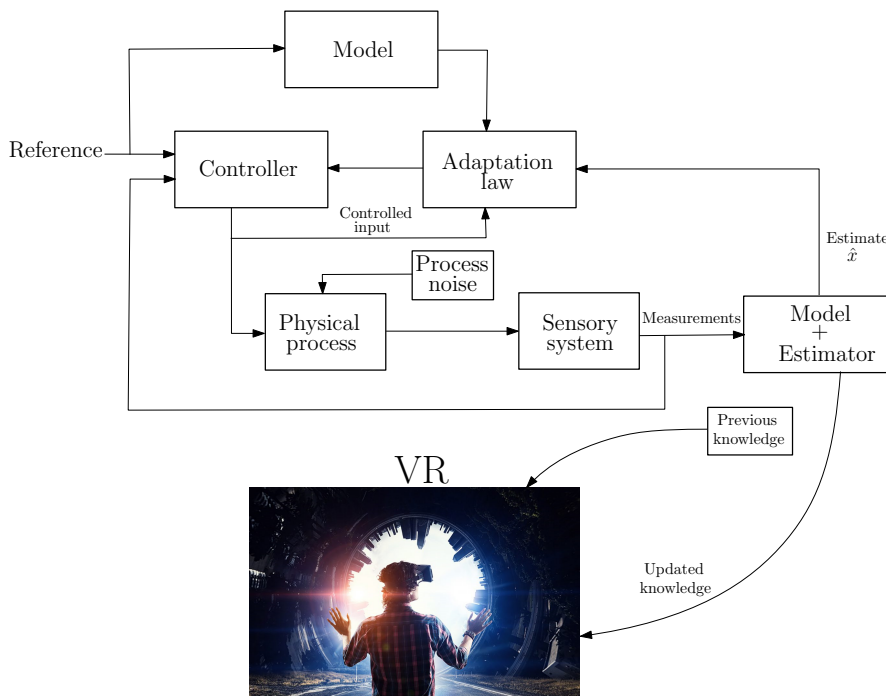


Figure 3.4: Adaptive control scheme with VR.

3.3.1 Least square

Any model that is linear in the parameters θ_i , can be written as a linear regression:

$$\begin{aligned} y_i &= \phi_1(x_i)\theta_1 + \dots + \phi_n(x_i)\theta_n + e_i = \\ &= \phi^T \theta + e \end{aligned} \quad (3.12)$$

where:

- $y = [y_1, \dots, y_N]^T$ is the measured output vector, function of the observable states x_k ;
- $e = [e_1, \dots, e_N]^T$ is the error vector. It takes into account the uncertainties in θ ;
- $\theta = [\theta_1, \dots, \theta_N]^T$ is the parameter vector;
- $\phi = [\phi_1, \dots, \phi_N]^T$ is the regression vector;

Therefore, this estimation problem aims to estimate -offline- the vector $\hat{\theta}$ when some cost function of $V(e)$ is minimised (for a more detailed analysis, the interested reader should take a look at (Ljung, 1998)).

If $\phi^T \phi$ exists and it is non singular, the parameter vector is the unique solution:

$$\hat{\theta} = (\phi^T \phi)^{-1} \phi^T y \quad (3.13)$$

3.3.2 Recursive least square

When the interest moves to estimate in real time θ , in other words updating θ_{i-1} when the values $\{y_i, x_i\}$ are measured, then a recursive formulation is needed.

Ljung et al., in ([Ljung, 1998](#)), illustrated how to use the *inversion lemma* to accomplish so, elegantly demonstrating that the online estimated parameters $\hat{\theta}_i$ can be evaluated by:

$$\hat{\theta}_i = \hat{\theta}_{i-1} + K_i (y_i - \phi_i^T \hat{\theta}_{i-1}) \quad (3.14)$$

$$\text{where } \begin{cases} K_i = P_{i-1} \phi_i (1 + \phi_i^T P_{i-1} \phi_i)^{-1} \\ P_i = (I_n - K_i \phi_i^T) P_{i-1} \end{cases} \quad (3.15)$$

From equation 3.14, it is worth noting that the new estimate $\hat{\theta}_i$ is equal to the previously evaluated ($\hat{\theta}_{i-1}$) corrected by the term $(y_i - \phi_i^T \hat{\theta}_{i-1})$, i.e. the single-step prediction at the time $(i - 1)$.

Moreover, the initialisation problem for P_0 (equation 3.15) can be dealt by admitting a small initial error $\epsilon \ll 1$ such that $P_0 = \frac{1}{\epsilon} I_n$. Besides, a variation of the RLS method, namely exponentially weighted recursive least square (EWRLS) can help to deal with varying parameters ([Love and Book, 2004](#); [Erickson et al., 2003](#)). It can be achieved by tuning w_i inside the expression of the cost function $V(e_i) = \sum_{i=1}^N w_i e_i^2$, therefore the covariance matrix P_i , so as to value more the latest measurements w.r.t. the older ones ([Biagiotti and Melchiorri, 2007](#)). This new recursive formulation is therefore reported beneath:

$$\begin{cases} \hat{\theta}_i = \hat{\theta}_{i-1} + K_i (y_i - \phi_i^T \hat{\theta}_{i-1}) \\ K_i = P_{i-1} \phi_i (\beta + \phi_i^T P_{i-1} \phi_i)^{-1} \\ P_i = \frac{1}{\beta} (I_n - K_i \phi_i^T) P_{i-1} \end{cases} \quad (3.16)$$

where the forgetting factor $\beta \in [0.95 - 1]$ takes care of these variations, the lower its value, the more the parameters varies.

3.3.3 Recursive Hunt-Crossley estimation

Using the Hunt-Crossley model (section 3.1.3), and assuming available force measurements as well as position and velocity and the end-effector, estimating the physical properties of the environment means finding the values $\{\hat{k}, \hat{d}, \hat{n}\}^2$.

Double stage identification

In ([Biagiotti and Melchiorri, 2007](#); [Diolaiti et al., 2005](#)) the author proposed a two stages RLS estimation by defining two estimators Γ_1 and Γ_2 as in figure 3.5. The vectors to applied the

²From now on, the suffix "i", indicating the sample time $t = iT$, will be omitted for simplicity.

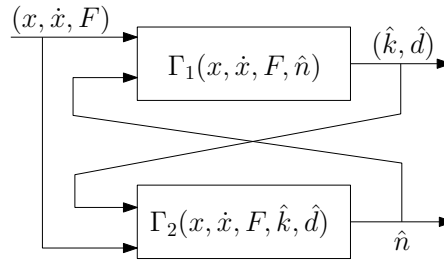


Figure 3.5: Online two stages estimation for the Hunt-Crossley model as in (Diolaiti et al., 2005).

recursive formulation 3.16 were defined as:

$$\Gamma_1: \begin{cases} \hat{\theta}_1 = [\hat{k}, \hat{d}]^T \\ \phi_1 = [x^n, x^n \dot{x}^n]^T \\ y_1 = [F_{HC}] \end{cases} \quad (3.17)$$

$$\Gamma_2: \begin{cases} \hat{\theta}_2 = [\hat{n}] \\ \phi_2 = [\log(x)] \\ y_2 = \left[\log\left(\frac{F_{HC}}{k + d \dot{x}}\right) \right] \end{cases} \quad (3.18)$$

This method has experimentally proved to be sound: convergence to the true values is obtained under strict assumptions about the nature of the error, material properties and initial values for the estimates $\hat{\theta}_i$ while using an had-hoc forgetting factor β .

Single stage identification

In (Haddadi and Hashtrudi-Zaad, 2008), Haddadi et al. presented a novel way to estimate recursively the parameters of the Hunt-Crossley model using a one-step procedure. A thorough analysis about the weaknesses of the previously two-stages method revealed that although it leads to convergence, it is very sensitive to parameter initial conditions and dynamic properties variations.

Recalling equation 3.9, for $x > 0$ it has been shown that:

$$F_{HC}(t) = k x(t)^n + d \dot{x}(t) x(t)^n + \epsilon \quad (3.19)$$

where ϵ is the process noise. Clearly, the RLS cannot be straightly applied to such a non-linear system.

From equation 3.19, the readers will agree on the equivalence³:

$$\begin{aligned} \ln(F_{HC}) &= \ln \left[kx^n \left(1 + \frac{d\dot{x}}{k} + \frac{\epsilon}{kx^n} \right) \right] = \\ &= \ln(k) + n \ln(x) + \underbrace{\ln \left(1 + \frac{d\dot{x}}{k} + \frac{\epsilon}{kx^n} \right)}_{1+\alpha} \end{aligned} \quad (3.20)$$

With the aim to linearize equation 3.19, the Maclaurin expansion $\ln(1 + \alpha) \rightarrow \alpha + O(\alpha^2)$ if $\alpha \rightarrow 0$, could be a tool. Hence, it has to hold that:

$$|\alpha| = \left| \frac{d\dot{x}}{k} + \frac{\epsilon}{kx^n} \right| \leq \left| \frac{d\dot{x}}{k} \right| + \left| \frac{\epsilon}{kx^n} \right| \rightarrow 0 \quad (3.21)$$

The last inequality implies that both the terms $\left| \frac{d\dot{x}}{k} \right|$ and $\left| \frac{\epsilon}{kx^n} \right|$ should be "small enough". As a rule of thumb, the former can be solved bounding the velocity to the condition:

$$\|\dot{x}\|_{\infty} < 0.1 \frac{k}{d} \quad (3.22)$$

On the other hand, the latter can be overcome by fixing a minimum penetration so as to satisfy for example:

$$\|x^n\|_{\infty} > B \frac{\epsilon}{k} \quad (3.23)$$

where the constant B has to be ≥ 10 , in order to neglect the process noise term in equation 3.19.

As a matter of fact, both these conditions depends on the properties of the environment and on the power of noise. Although both reasonably achievable, they have to be checked within the experimental phase.

Upon the above constraints, equation 3.19 becomes:

$$\ln(F_{HC}) = \ln(k) + n \ln(x) + \frac{d\dot{x}}{k} \quad (3.24)$$

hence a linear system, and the EWRLS estimation (equations 3.16) can be applied using the vectors:

$$\begin{aligned} \hat{\theta} &= \left[\ln(\hat{k}), \frac{\hat{d}}{\hat{k}}, \hat{n} \right]^T \\ \phi &= [1, \dot{x}, \ln(x)]^T \\ y &= [\log(F_{HC})] \end{aligned} \quad (3.25)$$

This method has been experimentally validated in (Haddadi and Hashtrudi-Zaad, 2012) and its superiority w.r.t. the two stages procedure proved.

³The time dependency has been left out for clearness.

3.3.4 Friction coefficients estimation

From the linear model 3.11, and using the same nomenclature as in section 3.3.1, the following vectors are defined :

$$\begin{aligned}\hat{\theta} &= [\hat{\mu}_{st}, \hat{\mu}_{kin}]^T \\ \phi &= [F_x, \dot{y}]^T \\ y &= [F_y]\end{aligned}\tag{3.26}$$

The same can be used to run a RLS estimation, i.e. equation 3.16.

Persistent excitation

To achieve the convergence of $\hat{\theta}$ to the true value(s), an important role is played by the richness of the input signal to the process. This concept, more commonly referred to as persistence of excitation (PE), stands to express the qualitative notion that the input signal to the plant should be such that all the modes of the plant are excited ([Narendra and Annaswamy, 2012](#)).

Specifically to the above mentioned case, three parameters have to be estimated $(\hat{k}, \hat{d}, \hat{n})$, hence as a rule of thumb ([Slotine and Li, 1989](#)), a reference signal containing two sine functions should be enough. However, the non linearity effect due to the logarithmic function in 3.24, should lead to convergence already with a single periodic reference signal ([Haddadi and Hashtrudi-Zaad, 2012](#)). These claim has been confirmed in ([Yamamoto et al., 2008](#)), where the authors compared three different level of excitation so as to determine the minimal requirement for convergence: one sine function turn out to be enough.

In ([Misra and Okamura, 2006](#)), Misra et al., showed how to ensured PE by adding high-frequency vibrations to the reference signal, later on removed by filtering to meet the transparency requirements.

4 Design and implementation

4.1 Simulations

From a feasibility aspect, simulations are carried out to confirm the allegations from the previous chapters. Firstly, simulations have been carried out using constant parameters $K(t)$, $B(t)$ and n , where the estimated values immediately converged to the real ones. Because of that, other simulations have been made more realistic considering varying physical properties (linearly w.r.t. the simulation time), such that:

$$K(t) = 100 + 10 t$$

$$B(t) = 10 + 1 t$$

$$n = 1.2$$

Besides, in order to make the input signal a persistent excitation, a multi-sine reference established the interaction along the perpendicular direction in between the end-effector of the robot and the real environment, as it follows:

$$z(t) = 0.012 \sin(2\pi 2 t) + 0.003 \sin(2\pi 5 t) + 0.021$$

Figure 4.1 reports the imposed kinematics of the end-effector, meant to represent the punctual trajectory of it as it was translating along the z-axis. The last terms guarantees that $z(t) > 0 \forall t$, i.e. a superimposed contact, while two modes of the environment are excited. Additionally, to make the simulation more realistic, a white noise with $SNR = 40$ enriches the frequency content of the reference signal $z(t)$. For the sake of curiosity, the FFT of $z(t)$ has been attached into the appendix figure A.1.

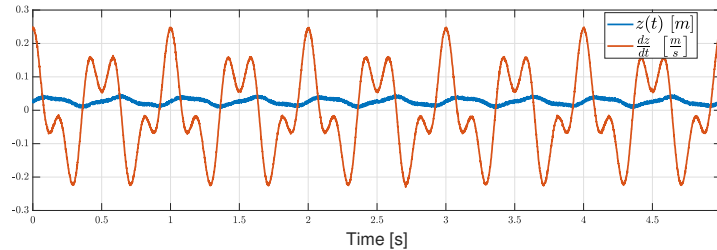


Figure 4.1: Simulations: reference kinematics.

4.2 Experimental phase

In a nutshell, since the problem in hand involves commanding a specific kinematics to the end-effector of the robot, together with measuring reaction forces to fit a specific physical model, a position-controlled robotic arm would be a natural choice. However, due to practical circumstances, an already existing set-up (Nijof, 2018) employing an impedance controlled (section 2.1) robotic manipulator by Kuka (section 2.4 for details) has been used. Hence, the highest possible value for the stiffness of the controller, so as not to experience

instability, has been set.

As a matter of fact, although this precautionary measure, the robot has behaved in a rather soft manner, potentially far away from an position controlled setup: the consequences of that will be clarified within the following sections.

4.2.1 Methodology

From the previous chapter, referring to figure 4.2, this research aims to achieve the mapping:

$$M_p := \{\hat{K}, \hat{B}, \hat{n}, \hat{\mu}_{st}, \hat{\mu}_{kin}\} \forall \Phi_0 P_{i,j} \quad (4.1)$$

With this goal in mind, the end-effector of the slave robot will "scan" the environment in

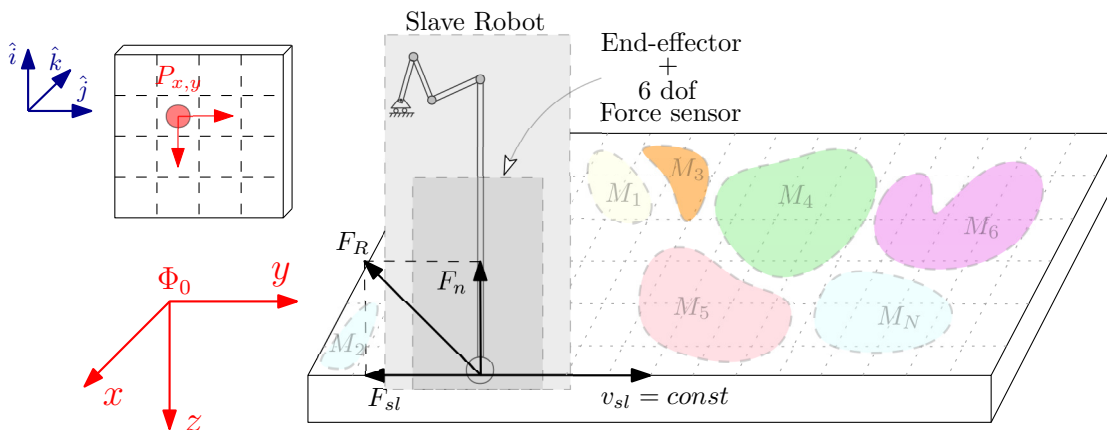


Figure 4.2: Procedure and physical properties mapping.

order to evaluate its physical properties, namely stiffness K and damping coefficient B , the adimensional n (only for HC model) and the friction parameters μ_{st} and μ_{kin} , all function of the only planar coordinates (x, y) ¹.

For the purpose of estimating K and B , perpendicularly w.r.t. A (figure 3.1), the end-effector of the robotic manipulator will interact with the real environment by means of an orthogonal poking motion: i.e. a punctual excitation. From that, the triad \hat{K} , \hat{B} and \hat{n} or the pair \hat{K} , \hat{B} will be evaluate using the HC and/or KV contact model, respectively.

Such an approach will be iteratively repeated a sufficient number of times N , so as to end up with N triads \hat{K} , \hat{B} and \hat{n} or the pairs \hat{K} , \hat{B} .

On the other hand, another trajectory will be commanded to the Kuka arm to estimate the friction coefficients μ_{st} and μ_{kin} in between the tip of the end-effector and the surface-planar, for simplicity- of the environment, sliding from one point to another (figure 4.6). For instance, once the static value of the friction is overcome, the end effector will start sliding upon the surface, maintaining a constant penetration $z(t)$ and velocity $v_{sl}(t)$. At this point,

¹This dependency, for simplicity, will be assumed implicit and not further reported.

the two dynamics of poking and sliding, although coupled, can be in part associated to the normal $F_n(t)$ and planar $F_{sl}(t)$ components of the measured $F_R(t)$ respectively. Under this conditions, and within the kinetic range of friction (section 3.2), both F_n and F_{sl} are expected to be overall constant; if it is not the case, at least one of the previous estimates changes value, i.e. the material properties are discontinuous. Hence, by uniquely monitoring the evolution of F_n and F_{sl} during such a gliding, one can get a grasp about when/where the RE changes its physical properties.

4.3 Experiment design

4.3.1 Elastic environment

The easiest tested scenario has been a, allegedly, chiefly elastic environment: for instance, a tense elastic band has been attached at the tip of the end-effector, in line with the poking direction and perpendicularly w.r.t. the ground (figure 4.3). Insightful outcomes

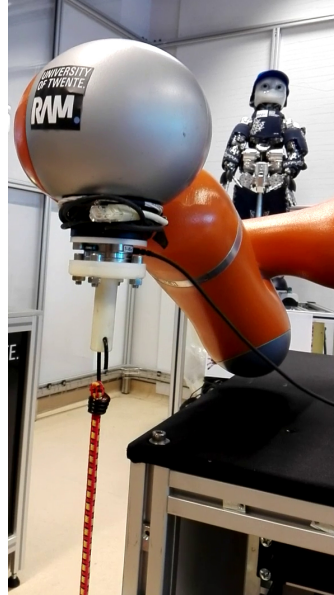


Figure 4.3: KUKA arm interacting with an elastic environment.

about the setup limits, models complexity, and estimation procedure turn out by means of experimenting onto this *quasi*-elastic environment. As a matter of fact, from a trivial static experiment, and applying Hooke's law, the expected stiffness of the band was around $88 \frac{N}{m}$. Subsequently, in order to estimates the longitudinal properties of the RE, the elastic has been pretensioned to such an extent that for the minimum elongation ($0.045 m$), a residual tensile stress was still present (no flaccid behaviour).

In the end-effector coordinates, the commanded displacements obeyed to the relation:

$$\begin{aligned} x(t) &= 0 \\ y(t) &= 0 \\ z(t) &= 0.025 \sin(2\pi 1.7 t) + 0.010 \sin(2\pi 4 t) + 0.08 \end{aligned} \tag{4.2}$$

However, even though the short stroke and the soft environment, poor tracking performance of the employed setup were evident. For the sake of thoroughness, figure 4.4 demonstrates this observation, while it is worth mentioning that it does not represent a real problem since the goal of this research differs from fine manipulative tasks.

While the elastic force exerted by the environment would push the end-effector's tip toward

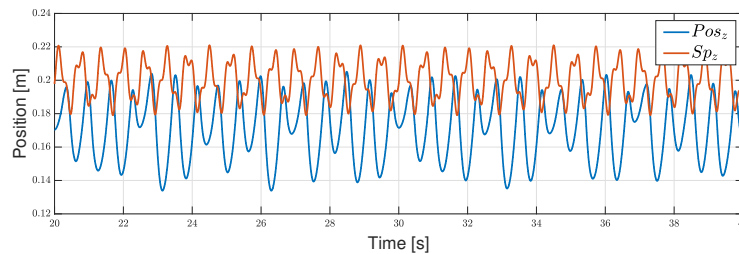


Figure 4.4: Elastic environment: position set-point tracking.

the negative direction, the robot does not apply enough torques to reach the higher $z(t)$. From that, it is obvious the existing trade-off among the level of pretension (F_e) and the tracking performance. While the latter does not affect the models fitting (positions and forces are still available), it turns out to be trickier to reach a persistent excitation, as needed to perform an online estimation (section 3.3.4).

4.3.2 Viscoelastic environment I: anechoic sponge

A similar set of experiments as for the *quasi* elastic environment have been carried out using a anechoic sponge (figure 4.5a) to mimic another kind of plausible RE scenario. Furthermore, the experimental procedure has been standardised for both the poking and sliding movements - not integrated but independently executed - as it follows:

- **Phase I** - the tip of the end effector slowly moves closer to the material surface and penetrates the material for the desired depth (constant velocity phase, lasting ≈ 5 s);
- **Phase II** - a standing phase (null velocity, lasting ≈ 1 s) has been placed so as to get rid during the data processing phase of possible bias in the force sensor measurements, prior the experiments start;
- **Phase III** - poking or sliding motion, depending on the wanted properties, takes place following specific commanded trajectories;
- **Phase IV** - phase I is reversed and the residual penetration is removed ($z(t) = 0$);
- **Phase V** - the original position is reached (x_0/y_0 , only for sliding).

Poking

Following the just mentioned experimental outline, a reference position as in equation 4.3 is commanded to the robot (in end-effector coordinates) during phase III. For the sake of

completeness, the interaction took place at the geometric centre of the surface ($4 \times 4 \text{ cm}$) of the rubber.

$$\begin{aligned} x(t) &= 0 \\ y(t) &= 0 \\ z(t) &= 0.003 \sin(2\pi 0.9 t) + 0.001 \sin(2\pi 5 t) + 0.012 \end{aligned} \quad (4.3)$$

Sliding

In order to observe a behaviour similar to figure 3.3a, the friction coefficients determination is based on the assumptions that the penetration inside the material is constant. For instance, w.r.t. the material surface, the following motion profile - during phase III - is commanded:

$$\begin{aligned} x(t) &= 0 \\ y(t) &= 0.003 t \\ z(t) &= -0.0025 \end{aligned} \quad (4.4)$$

Moreover, during this phase, a constant orientation is imposed to the last joint of the robot, viz. the end effector is always perpendicular w.r.t. the material surface.

4.3.3 Viscoelastic environment II: smooth-on Ecoflex 50

Thus, in order to have a larger population of tested materials (mimicking different RE scenarios), the rubber -silicon type- *Ecoflex 50*², produced by Smooth-On, has been tested as in the previous case. Because of its low viscosity, softness and stretchy properties, it is often used to make prosthetic appliances and cushioning for orthotics. For purposes which will be clearer later, nonetheless, the sample has been coloured with red glitter (figure 4.5b). It is worth pointing out that due to the higher stiffness of this RE, only smaller penetration was possible ($< 1 \text{ cm}$), *de facto* making harder reaching a PE to recursively estimate the coefficients of the HC model. The considered reference signal was:

$$\begin{aligned} x(t) &= 0 \\ y(t) &= 0 \\ z(t) &= 0.0015 \sin(2\pi 0.9 t) + 0.0005 \sin(2\pi 5 t) + 0.003 \end{aligned} \quad (4.5)$$

4.3.4 Viscoelastic environment III: smooth-on Dragon skin 10

Eventually, another silicone compound used for a variety of applications, ranging from creating skin effects to making production molds, has been employed as a RE sample: the *Dragon skin 10*³ produced by Smooth-On. From specs, this silicone is slightly stiffer than the previous one; nonetheless, to better distinguish it from the other rubber type, it has been coloured with blue glitter (figure 4.5c).

²Shore hardness: 00-50

³Shore hardness: 10 A



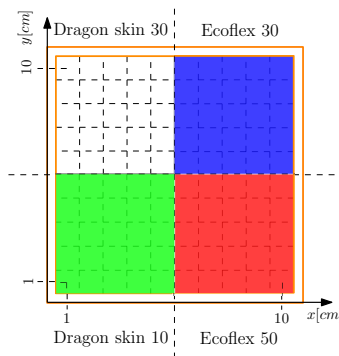
(a) Anechoic sponge.



(b) Ecoflex 50.



(c) Dragon skin 10.



(d) Ideal mixed environment.



(e) Real mixed environment.



(f) Overflowed layers.

Figure 4.5: Experimented types of real environments.

4.3.5 Mixed environment

Using the previous cases as test bench, and the corresponding outcome as a reference, a mixed RE has been prepared by placing four different types of rubbers within a square mold (figures 4.5d). Approximately each quarter of it has been filled with a liquid compound, differently coloured, as it follows:

- *Ecoflex 30*⁴ - blue;
- *Dragon skin 30*⁵ - white;
- *Ecoflex 50* - red glitter;
- *Dragon skin 10* - green glitter.

During the preparation, due to the different viscosity of the liquids, the compounds slightly mixed up, making the RE even more interesting: in particular, the blue *Ecoflex 30* (out of all, the softest silicone from specifications) overflowed upon the *Dragon skin 30* (the stiffest one, on paper). Figures 4.5e and 4.5f show this effect into the final solid compound.

Poking

A grid with 10x10 little squares, meshed using 1x1 cm links, has been virtually drawn to carry out 100 point-wise poking procedures, to partially estimate the mapping M_p of this mixed RE. From those experiments, the effect of the "rigid" border of the mold, and an ambiguous behaviour due to the mixed fluids are expected to arise during the data processing phase.

Sliding

Figure 4.6 shows the paths which have been followed by the probe to determine if any force leap occurs when sliding upon the RE's surface. In particular, the bold and labelled arrows are used as the representative trajectory to shows the most relevant transitional behaviours from one type of silicone to the other. During this gliding phase, the set-point trajectory of the probe obeyed to the relations:

$$\begin{array}{rcl}
 x(t) = 0 & & x(t) = -0.002 t \\
 y(t) = 0.002 t & \text{or} & y(t) = 0 \\
 z(t) = -0.0025 & & z(t) = -0.0025
 \end{array} \tag{4.6}$$

depending on the direction of the sliding, as sketched in figure 4.6. Moreover, during this phase, a constant orientation is imposed to the last joint of the robot, viz. the end effector is always perpendicular w.r.t. the material surface.

⁴Shore hardness: 00-30

⁵Shore hardness: 30 A

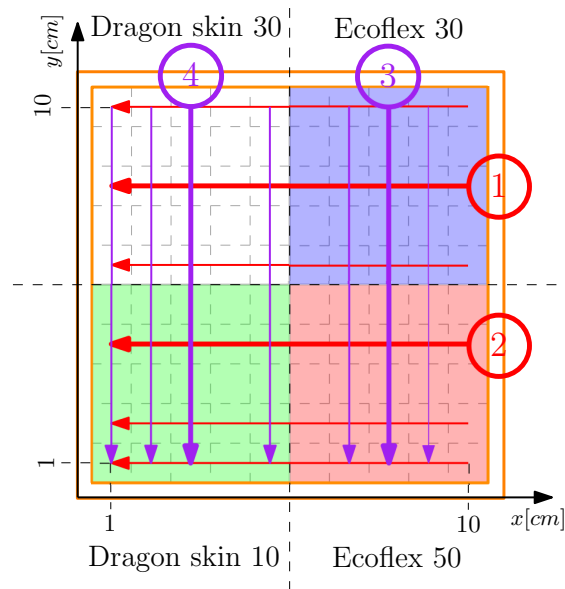


Figure 4.6: Mixed environment: grid and sliding paths.

4.4 Visual identification

Within this section, an hint to the recognition of the physical properties of the real environment via the only visual data is made. So far, the triad of values $M_p := \{\hat{K}, \hat{B}, \hat{\mu}_{eq}\}$ is aimed by enforcing the end effector of the robot to penetrate - up to a controlled extent - the surface of the real environment. Such a situation, however, is not always feasible and it can be a risk when dealing with fragile or exploding environments, for example. Furthermore, as described in the previous sections, evaluating the mapping M_p is a rather long-lasting procedure.

4.4.1 Concept

A picture taken from an RGB sensor camera, can be processed and classified considering the values of the three additive primary colours: red, green and blue. Referring to the sample of the mixed environment (section 4.3.5) addressed up until now, these components values are showed in figure 4.7.

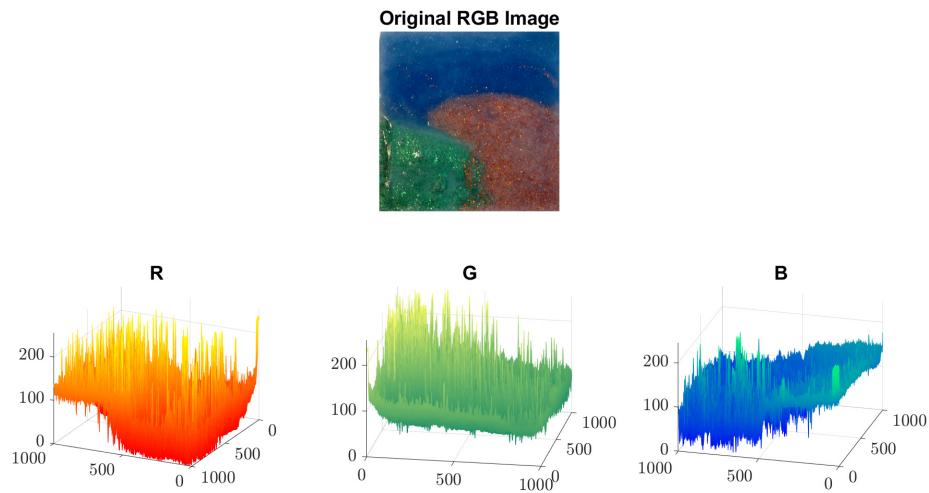


Figure 4.7: Mixed environment and its RGB components.

Since the mapping of the dynamic properties would be known, the aim is to train the system so as to immediately extract a first guess about the nature of these physical characteristics from the solely RGB image.

From this preamble, the following implication is investigated:

$$\{\hat{K}, \hat{B}, \hat{\mu}_{eq}\} \stackrel{?}{\leftrightarrow} \{R, G, B\}$$

$$\text{or } M_p \stackrel{?}{\leftrightarrow} M_v$$

5 Results

This chapter outlines the results of this research, as they can be inferred from the outcome of the experiments as described in the previous chapter.

5.1 Simulations

Accordingly to figure 5.1, the force components of the HC model keep a positive sign, while the viscous contribution is greatly minimised w.r.t. the the same term into the KV representation. Moreover, looking at the same plots, it stands clearly how much smaller was the damping component of the HC model (negligible in this case) w.r.t. the KV description.

On the other hand, as it was predictable from the observations of section 3.1.2, negative F_B

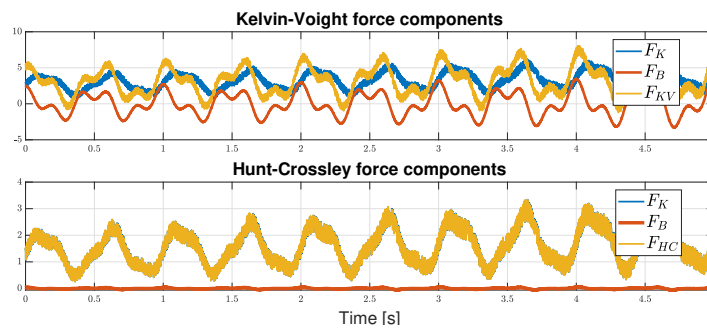


Figure 5.1: Simulations: forces components of the KV and HC models.

arises in the KV model, and this physical inconsistency is even more evident looking at the energy hysteresis diagram in figure 5.2.

It has been straightforward estimating \hat{K} and \hat{B} for the KV model, using the RLS procedure:

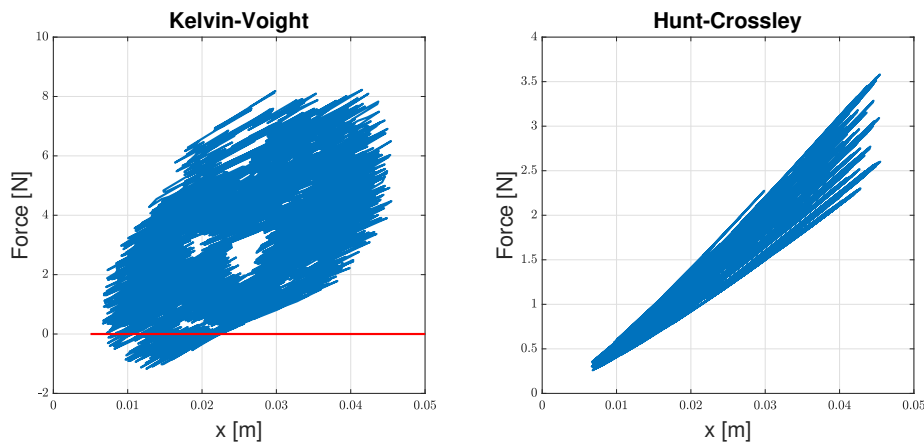


Figure 5.2: Simulations: energy hysteresis diagrams.

for instance, already with a constant forgetting factor $\beta = 0.98$, the method yields to an

immediate ($< 0.1s$) convergence of the parameter vector $\hat{\theta}$ to the simulated values. More interesting is the recursive estimation for the linearized HC model: figure 5.3 displays the outcome.

In this case, using $\beta = 0.98$ or an exponentially weighted $\beta = 1 - 0.01 e^{-5(t-2)}$ (section 3.3.3),

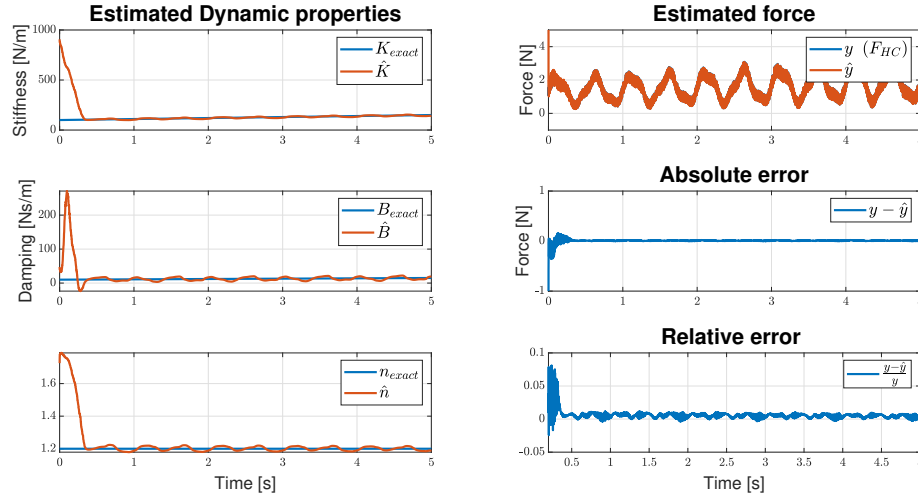


Figure 5.3: Simulations: EWRLS applied to the HC model.

does not show palpable differences (figure 5.3 illustrates the latter case). Here, the estimates converge to the simulated values after 0.3 s with some bland LF oscillation (variation $\leq 1.5\%$).

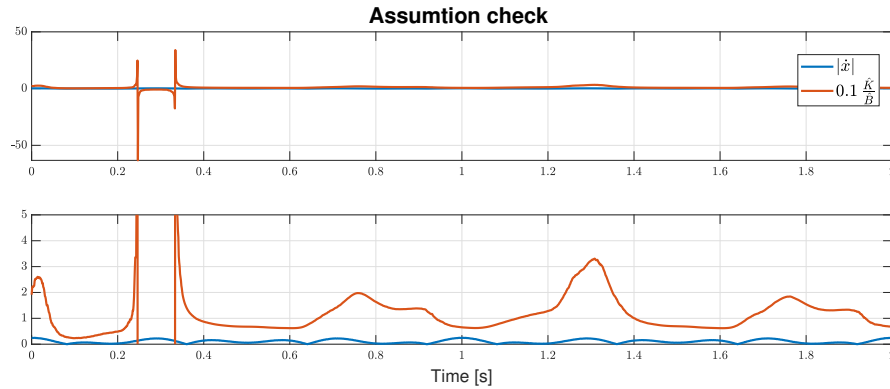


Figure 5.4: Simulations: assumption validity check for the linearized HC model.

This result is anyway subjected to the validity condition given by equation 3.22, relatively to a consistent estimate: hence, figure 5.4 proves that after 0.33s the linearized HC model (eq. 3.24) is a valid approximation of the non linear one (eq. 3.19), that is $\|\dot{x}\|_{\infty} < 0.1 \frac{k}{b}$.

5.2 Experiments

5.2.1 Elastic environment

The plots in figure 5.5 show the measured positions and forces when the robot interacts with an (chiefly) elastic RE. As an evidence of the *quasi* elasticity of the environment, the third plot

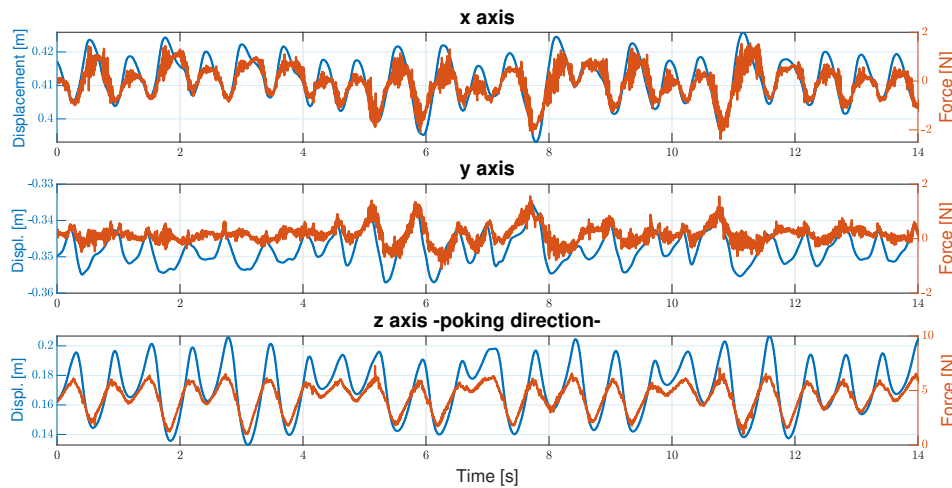


Figure 5.5: Elastic environment: measured forces and positions.

suggests the *quasi* linear relation position/force. However, from the same figure, an evident coupling among the axis arises: along the x and y directions, in fact, displacements (and consequently forces) occur, contrary to the set-points 4.2.

As for the simulated case, applying a RLS to the KV model with $\beta = 0.98$, led straightforwardly

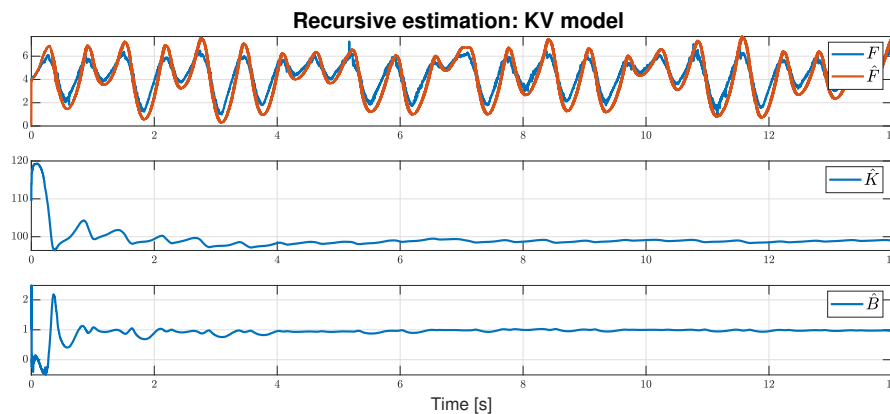


Figure 5.6: Elastic environment: online estimation KV model.

to convergent estimates, plotted in figure 5.7 and summarised in table 5.1; moreover, this model showed mild sensitivity to the frequency content of the reference signal (i.e. always persistently exciting). On the other hand, the HC model converged with an EWRLS (section

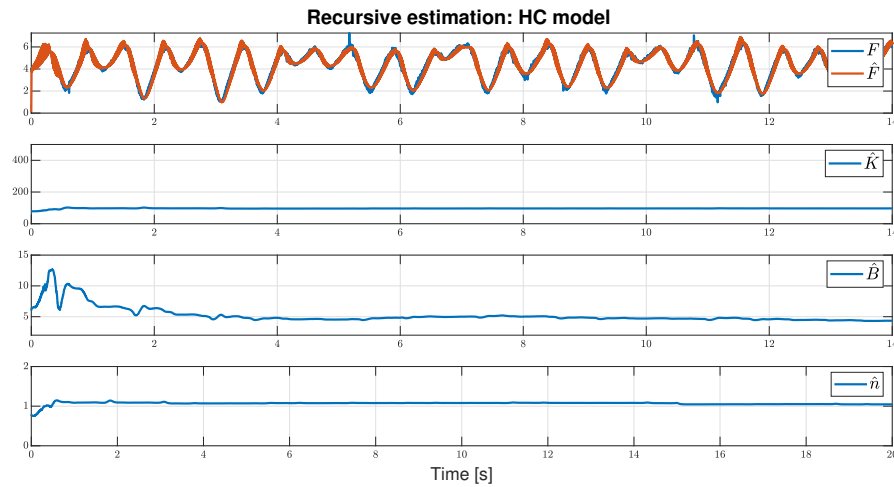


Figure 5.7: Elastic environment: online estimation HC model.

3.3.3), choosing $\beta = 1 - 0.01 e^{-3(t-2)}$ to balance the convergence with the time to reach it. For such a soft environment, however, a PE has been possible by increasing the amplitude of the components of $z(t)$ in 4.2, an unfeasible instance if the RE were stiffer though.

Furthermore, for the sake of consistency, the linearization validity has been checked and reported in the appendix figure A.3. Eventually, the output estimates from both the models

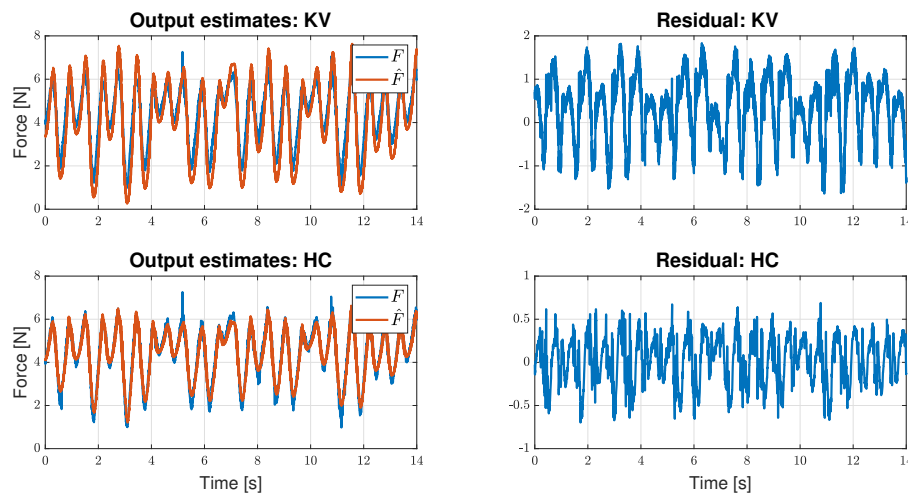


Figure 5.8: Elastic environment: estimates' residual.

are compared in figure 5.8, and the residual $\sigma = y - \hat{y}$ evaluated. As a measure of estimation performance, the subtended area (viz. the integral) of the residuals has been computed and reported into the table 5.1. The values confirm the theory presented in chapter 3: in fact, in

spite of the higher complexity, the one-stage recursive estimation of the HC model performs better than the KV one for such a soft material.

Model	\hat{K} [$\frac{N}{m}$]	\hat{B} [$\frac{Ns}{m}$]	\hat{n}	$\int \sigma$ [Ns]
Hooke	99.43	\times	\times	14.98
Kelvin-Voight	98.12	0.96	\times	12.85
Hunt-Crossley	92.52	3.37	1.028	4.42

Table 5.1: Elastic environment: models' estimates.

Following a large number of experiments (> 100), and using the maximum allowed value for the impedance of the controller ($K_c = 5200$), it has been observed that the robot was not following the trajectory anymore whether the commanded motion had frequency components > 3 Hz. Moreover, as expected, the lower K_c , the worse the outcome: because of that, this weakness of the system has been associated to the implemented impedance controller.

Eventually, it can be stated that the tracking performance was inadequate when the highest frequency component of the set point 4.2 was > 3 Hz (i.e. the maximum BW of the robot). However, in this case, increasing the power content of the excitation (to achieve PE) has been possible by means of imposing a larger amplitude of the two sine components of $z(t)$ in equation 4.2. Clearly, such a large penetrations (≈ 0.035 m) would not be possible when dealing with stiffer RE - using the current set-up.

That been demonstrated, however, merely the KV model will be used further, due to the fact that hundreds of tests will be conducted and its simpler description allows a faster implementation, always keeping in mind the final goal: i.e. a 3D visual map of the dynamic properties of the RE. Moreover, it has been already mentioned that, with the employed experimental setup, achieving a persistent excitation is not either easy or always possible task. However, this choice is not a operational limitation: in fact, at this stage, the final operational scenario is not well defined yet, and this generalised framework overlooks from the assumed contact models and/or estimation techniques which, in turn, are always dependent on the application in hand.

5.2.2 Viscoelastic environment I: anechoic sponge

The estimates \hat{K} and \hat{B} when an anechoic sponge mimics the real environment have been obtained following the same procedure as before. Therefore, to streamline this report, the measured forces/positions and the estimation are attached within the appendix A.1.3 whereas the results are reported in table 5.2 for comparison with the other environment types.

Sliding

To evaluate the friction coefficients, an unidirectional sliding (lasting 10 s) as described by equations 4.4 has been completed. Figure 5.9 shows the results: although the reference 4.4 commands a constant penetration, it has been measured a $z(t)$ which changes over time and, in particular, it increases (bottom plot). As a consequence, the normal force F_n is not constant, and the planar component F_{sl} , in turn, ripples. From this evidence, it would be pointless talking about a static and/or kinematic friction coefficient because the boundary conditions change over time.

However, an equivalent friction constant μ_{eq} can be evaluated, when considering the only Coulomb's component of the model 3.11. The value of μ_{eq} has to be intended not as an absolute friction coefficient, whereas it is interpreted as a valuable generalised meaning to address the progressive slippage phenomena (Bicchi et al., 1993). Moreover, μ_{eq} depends on the elastic nature of the materials in contact, their geometry, on the extent of penetration and on the sliding velocity, among others variables.

A RLS estimation ($\beta = 0.98$) has been implemented as discussed in section 3.3.4 and the

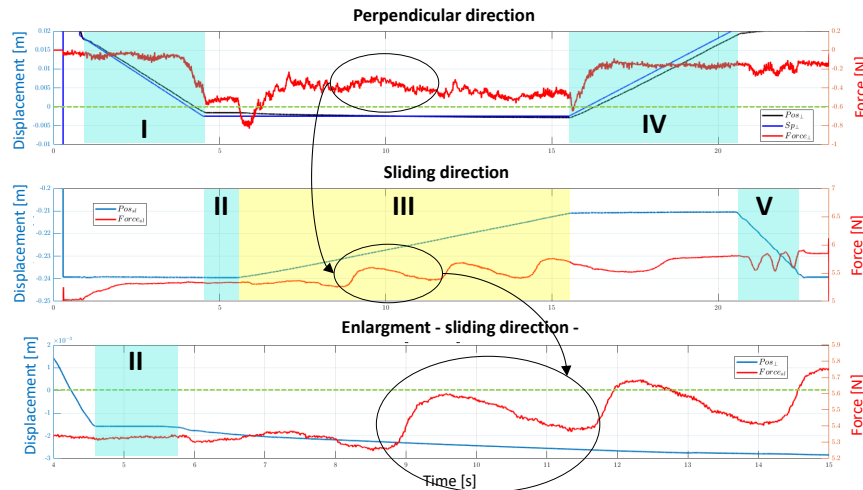


Figure 5.9: Spongy environment: sliding.

coefficients converges similarly to the previous estimations, reason why the plot has been attached into the appendix figure A.6. For the sake of completeness, the averaged converging value is reported in table 5.2.

5.2.3 Viscoelastic environment II & III

Following exactly the same methodology as for the anechoic sponge, the silicone samples of *Ecoflex 50* and *Dragon skin 10* have been characterised with a triad of values $M_p := \{\hat{K}, \hat{B}, \hat{\mu}_{eq}\}$ each. Details about the measured data are attached as appendices in A.1.4 and A.1.5, while the estimated value are reported in table 5.2 for comparison.

Environment type	\hat{K} $\left[\frac{N}{m}\right]$	\hat{B} $\left[\frac{Ns}{m}\right]$	$\hat{\mu}_{eq}$ []
Sponge	280	8.1	0.27
<i>Ecoflex 50</i>	732	9.9	0.82
<i>Dragon skin 10</i>	994	14.5	0.77

Table 5.2: Viscoelastic environments: estimates of some dynamic properties.

5.2.4 Mixed environment

Poking

When the mixed RE as described in section 4.3.5 has been addressed, the pair $\{\hat{K}, \hat{B}\}$ has been iteratively evaluated for each of the 100 square elements of the grid in figure 4.5d. As a result, these scattered data have been organised within a corresponding grid and, upon them, a surface has been fit using a biharmonic interpolation¹, as reported in figure 5.10. This distinction is even more evident interpolating using the nearest value, as in the appendix figure A.15. Such visual representations clearly indicate how the RE should dynamically behave, point by point. From that, four main zones are distinguishable, corresponding to the different silicone types exactly as one would infer from a "finger-touch" feeling (for the stiffness, at least). Moreover, the edges effect can be overall depicted by a damping increase and stiffness reduction, as expected from the common sense, due to the absence of supporting links at those points (e.g. glue or other neighbourhood materials).

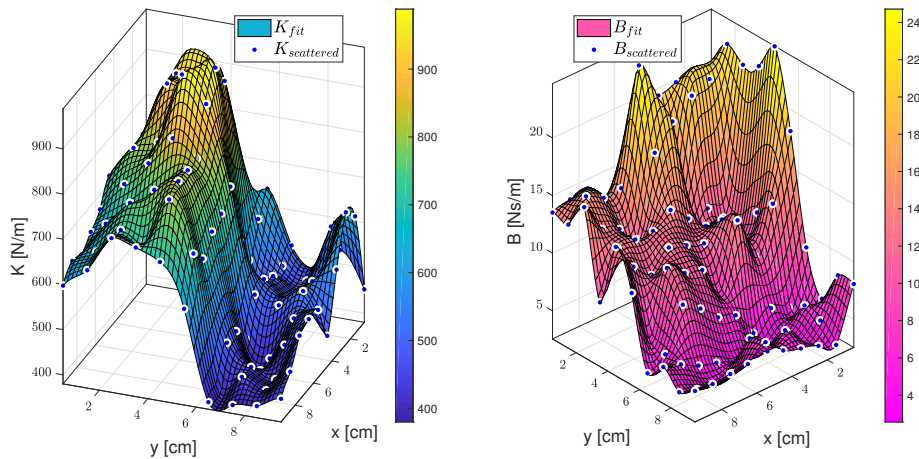


Figure 5.10: Mixed environment: estimated stiffness $K(x, y)$. Biharmonic interpolation.

¹Matlab reference [here](#)

Sliding

In order to prove the claim advocated in section 4.2.1, the set-point penetration of the probe inside the RE is kept constant during the sliding motion, and the three components of the forces, namely F_n , F_x and F_y are monitored. Therefore, the latter two are vectorially summed up and renamed as F_{sl} , to take into account for the contributions due to end-effector misalignment and/or deviation from the set point. Figures 5.11, 5.12, 5.13 and 5.14 show the evolution of positions and forces, relatively to the labelled paths into the grid 4.6.

From them, important conclusions can be drawn up:

- Path 1 does not allow to appreciate any change regarding the material properties. This outcome was expectable since the layer upon which the probe slides is made from the same silicone. Due to the minimal extent of penetration, the underlying layer of another type of silicone (clear from figure 4.5f) would not be recognisable;

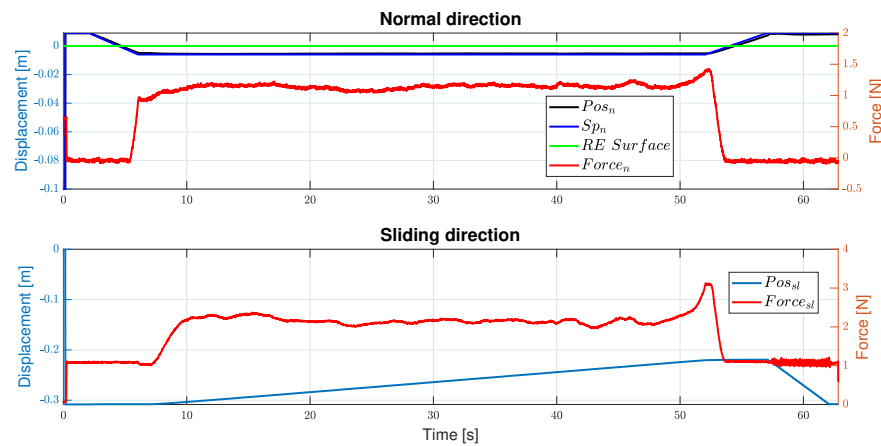


Figure 5.11: Mixed environment: sliding path 1.

- Path 2 show a steady change within the middle of the sliding pathway, corresponding to the transition area indeed. This result is also predictable looking at the respective mild changes of \hat{K} in figure 5.10;

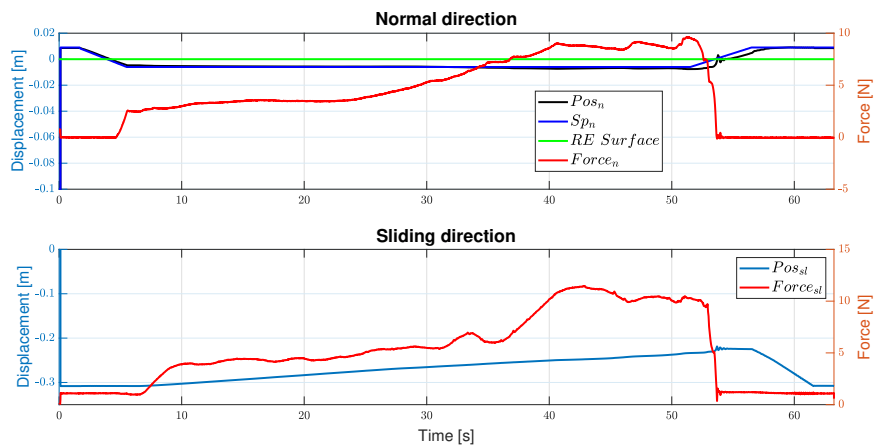


Figure 5.12: Mixed environment: sliding path 2.

- Path 3 points out how the monitored forces change when passing from the softest to the toughest area of the mixed real environment. This fact is evident from the abrupt jump, reaffirming the validity of the mapping;

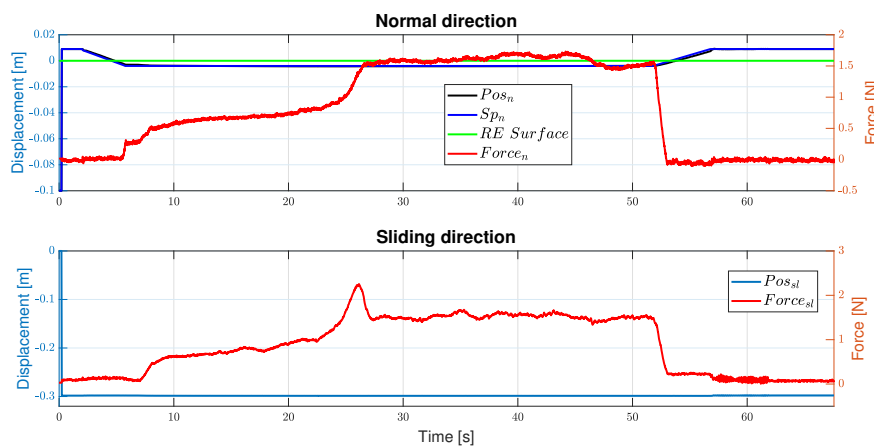


Figure 5.13: Mixed environment: sliding path 3.

- Path 4 can be similarly explained to the previous case, whereas the increase at the of the motion is bestowed on a defect of the surface.

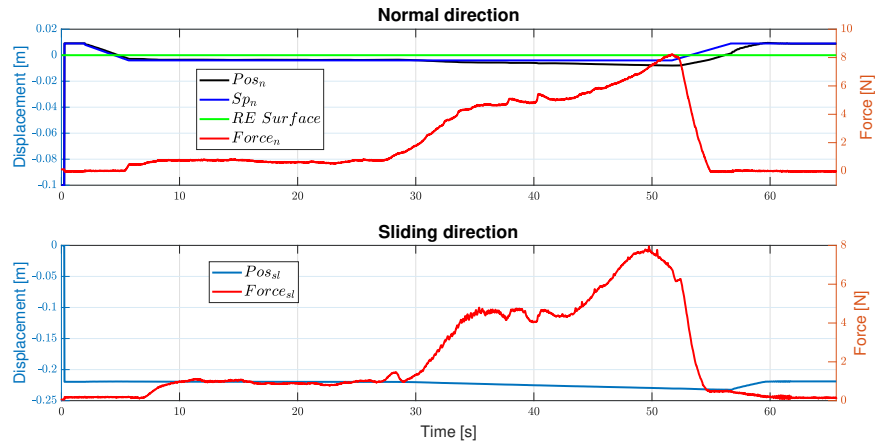


Figure 5.14: Mixed environment: sliding path 4.

5.3 Visual data

Herein, the only mapping of the stiffness K (figure 5.10) is considered as an illustrative case, since the procedure would be the same for B and μ_{eq} - all the properties are function of the planar coordinates x and y .

In particular, the correlation

$$\{R, G, B, \} \xrightarrow{?} \{\hat{K}\}$$

is sought.

5.3.1 Processing

In section 5.2.4 a 10×10 mapping of the stiffness has been evaluated and the values have been gathered under three classes (figure 5.15):

- Class 1: soft;
- Class 2: medium;
- Class 3: hard environment.

Supposedly, they are also representative of the three colours associated with the silicone types: *Ecoflex 30*, *Ecoflex 50* and *Dragon skin 10*, respectively. On the other hand, the RGB image of the silicone sample had a dimension 2512×2512 pixels.

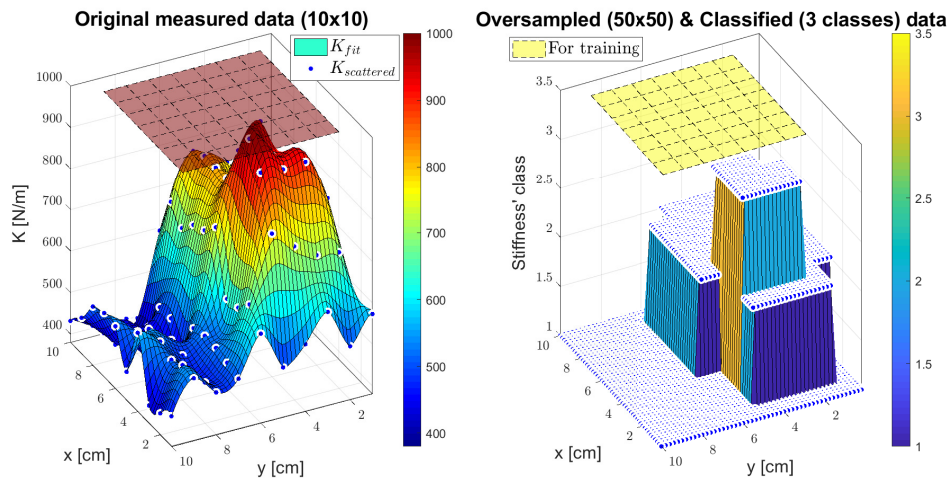


Figure 5.15: Mixed environment: stiffness classification.

The *Classification learner App*² by Matlab has been used for the purpose, and a dimensional coherency is needed to let the algorithm try to assign a class of K to a combination of values (or predictors) $\{R, G, B, \}$. Therefore, for this multi-class problem, the K -mapping has been oversampled (right plot in figure 5.15) to a $50 \times 50 \times 1$ array, whereas the predictors have been downsampled to a $50 \times 50 \times 3$ matrix, for dimensional compatibility - figure 5.16 shows the downsampled image.

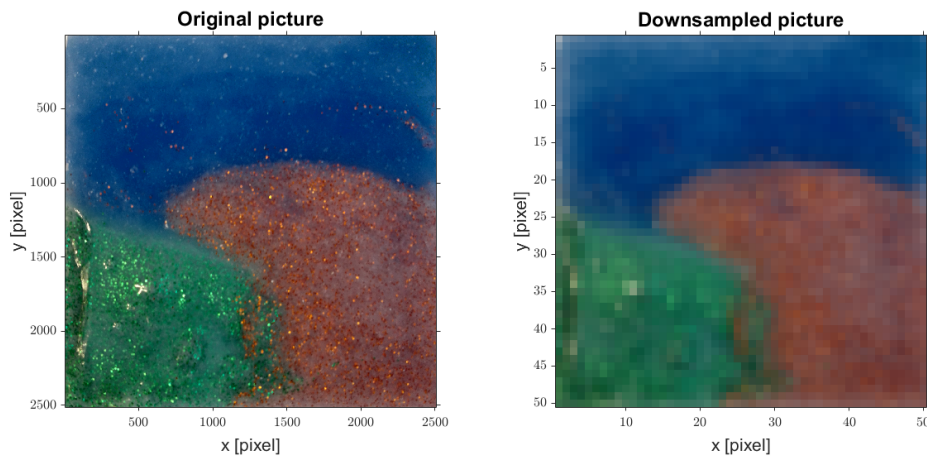


Figure 5.16: Mixed environment: downsampled image.

²Source: [website](#).

Within the *Classification learner App*, applying a cross-validation with 20 fold, and a Fine Gaussian SVM model, led to an accuracy of 80.3%. Therefore, this trained model has been used to predict the stiffness of the silicone samples in figures 4.5b and 4.5c. The outcome reported in figure 5.17 shows a perfect match (i.e. the predicted class is the expected one, based on the material properties) for the softest and toughest silicone, while some strayed peaks for the *Ecoflex 50* make the prediction less convincing.

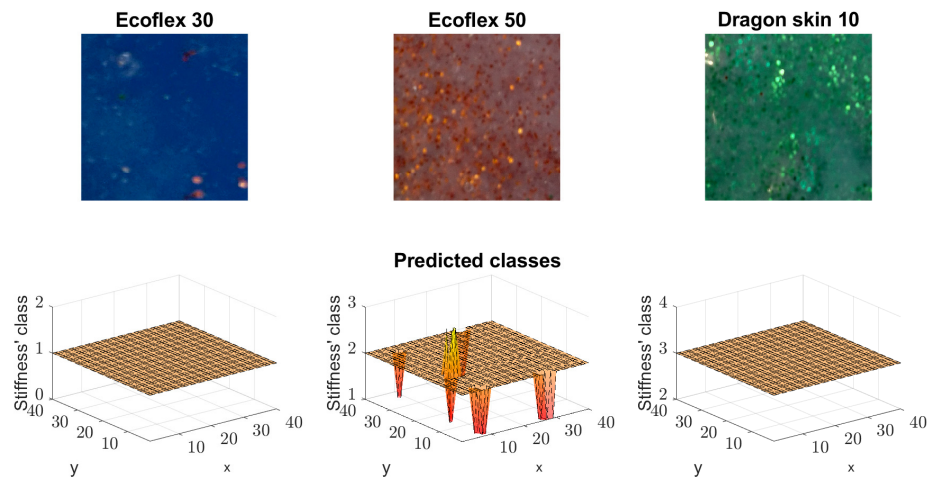


Figure 5.17: Predicted stiffness for the single silicone samples.

More interesting is the case reported in figure 5.18, where a second picture of the mixed environment has been used as input. Since the associated predictors are the same used for training, as expected, the outcome shows an accuracy around 81%.

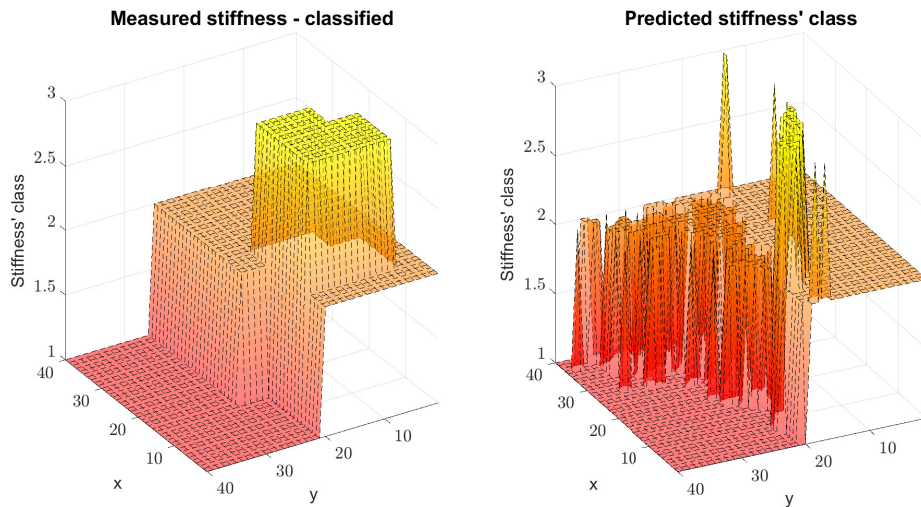


Figure 5.18: Mixed environment: predicted stiffness' class.

Eventually, one might conclude that, for a known environment there is a rather good chance (4 out of 5) to roughly identify its physical properties by only visual data. Although the presented simplistic case, it is still reasonable to envision an operational scenario that has recurrent patterns in terms of object, appearance and situations. From them, the system would learn and classify the surrounding so as to empower its autonomousness.

The author thinks that this approach would bring important advantages into the teloperation chain:

- avoid potentially destructive interaction with fragile/explosive environments;
- having an immediate first initial guess about the nature of the environment and its physical properties;
 - faster convergence of online estimation during interaction;
 - better adaptation of the haptic capabilities of the system.

6 Conclusions

A brief recap about the content of the previous chapters foreruns a critical interpretation of the results, while the last section leaves recommendations to pave the way to follow up this research.

6.1 Introduction

Chapter 1 introduced the topic of telemanipulation giving of it an historical background. It also brought evidences which lay dawn its relevance in present days and addressed its main shortcomings. For example, the importance of an upfront knowledge on the dynamic properties of the environment the robot interacts with has been discussed. Therefore, the i-Botics purpose has been explicated and, from that, the objective of this research clarified so as to make a step toward that higher-ranking goal. The following main research question has been posed:

How can a punctual estimation of the dynamic properties of the environment be extended into the 3D space, while employing a realistic multi-DOF robotic manipulator?

Subsequently, chapter 2 introduced the readers to relevant concepts regarding this field of research, so as to facilitate the overall comprehension of the text.

Then, following a meticulous literature review, chapter 3 presented different lumped contact models, generally used to mathematically describe the interaction in between the slave robot and the real environment. Therefore, under certain discussed assumptions, a linear recursive estimation method has been presented as a tempting candidate to evaluate on-line the dynamic properties of the approached object.

Chapter 4 began with numerical simulations, carried out to show the feasibility of the previously advocated theory. From that, an experimental procedure has been outlined, and tests conducted on different materials and *ad hoc* set-point trajectories.

As a result of these experiments, chapter 5 presented the arguments to answer positively to the research question, showing a spacial mapping of dynamic properties, namely stiffness, damping and friction coefficients. Moreover, a possible approach on how to combine the outcome from this research with visual data closed the chapter.

6.2 Findings and their implications

In conducting this research, as in a real operational scenario, a 7 *dof* Kuka robotic arm, free to move into the 3D space, interacted with an unknown surrounding. It is worth mentioning that the geometry and position of the collided object were known in advance; in fact, for simplicity, a planar surface has been considered. However, this assumption either represents a limitation or contradicts the obtained result: for instance, via the modern sensory capabilities and SLAM algorithms (Fuentes-Pacheco et al., 2015), reliable virtual 3D reconstructions and point clouds maps can be obtained for outdoor (Nüchter et al., 2007) and indoor (Henry et al., 2010) environments. Moreover, even though the impedance controller

which supervised the kinematics and dynamics of the Kuka has been proved not to be the best implementation for fine manipulative tasks, it generally represents the commonplace standard. The outcome would improve by means of using higher level of control, such as adaptive controllers and/or gain scheduling methods which should be placed side by side with the current implementation.

As a result of this automated interaction, estimates of the stiffness and damping coefficients of the "touched" points were available; hence, a spacial mapping of these properties has been built. This new description would enrich with physical meaning the available information about the environment, within its supposedly available virtual representation. In turn, it should allow the implementation of the impedance reflection method (section 2.2), proved to enhance the haptic performance of the system.

As a matter of fact, each estimation led to convergence after ≈ 3 s, where the initial values of the covariance matrix P (related to the first guess of the online estimator) was kept constant. In order to accelerate this type of recognition, an iteratively updating P with the previous estimates would likely lead to a faster convergence, whether the dynamic properties do not abruptly change. Furthermore, the studied silicone samples were overall soft type materials, and their physical properties into the same order of magnitude (relatively small variations); nonetheless, the result demonstrated an accurate classification and recognition of the even more peculiar characteristics of such an environment, e.g. border effects, inaccuracy of the surface or the overflowed silicone. From this considerations, the author believes that the same procedure would work even better within a real operational scenario, where these properties are likely to vary more (one could think to rocks or sand in undersea operations, to bring an extreme example). Besides, the robustness and stability of a telecontrolled system which interacts with a "rigid" real environment are assessment matters that the designer has to evaluate from time to time, based on the application in hand.

The visual part is trickier and, due to time constraints, it could not have been further explored within this research. The visual characteristics of a given scenario might lead astray if the only RGB information is considered: for instance, an homogeneously coloured soft covering would not reveal anything about the nature of the "hidden" layer(s). However, the author believes that by narrowing the focus on specific scenarios, more insightful knowledge can be gathered and classified; hence, it is very likely to happen that similar physical properties corresponds to the same RGB components. For example, if operating under water, basaltic rocks generally look like differently from coral sand, banally speaking. In any case, it would not be the only cue from which uniquely determinate the nature of the physical environment; nonetheless, it would still represent a valuable first guess for the above mentioned reasons (faster online estimation, above all).

6.3 Recommendations

Based on this work, the following recommendations are left as suggested paths for further developments on this topic. They are:

- investigating how these dynamic properties can be moved within a graphic engine (Gazebo or Unity, for example), and included into a virtual world in such a way haptic rendering was possible;
- conducting a thorough survey about safety. Contrary to the common affirmation "It's just a robot!", explosions and/or destruction are generally undesirable. Therefore, working toward a thorough recognition of the environment through information coming from contactless type sensors is recommended;
- automating such a recognition, making the human being only supervising the process and taking actions only when the system returns possible warning situations. In other words, increasing the AI role into the big picture;
- assessing the improvements (if any) by using this position dependant mapping of the impedance (as a generalised concept, namely both \hat{K} and \hat{B}) into an adaptive controller. It would immediately reflect the properties of the environment to the master and slave controllers, based only on position information of the end effector. In other words, implementing an *ultimate* impedance reflection method, which is independent from the elapsed convergence time. That is a scenario where the physical properties of the environment are known, nevertheless telemanipulative tasks are still needed due to its danger (e.g. chemical or nuclear industry);
- depending on the level of accuracy required for the mapping M , one could opt to carry out a point-wise estimation only when a reasonable jump in F_n or F_{sl} is measured, accelerating the entire estimation procedure. For example, it might be done by tuning an allowable threshold for $\frac{\delta F_n}{\delta x}, \frac{\delta F_n}{\delta y}$ and $\frac{\delta F_{sl}}{\delta x}, \frac{\delta F_{sl}}{\delta y}$, so that only when exceeded, a new estimation would adequately update the previous values;
- even though it lies beyond the field of telerobotics, it might be interesting exploring the conception of a probe which was able to determine the geometry (as the on current 3D scanners) and the dynamic properties of the scanned object. That is embedding the latter capability into the currently commercialised 3D-probes.

6.4 Conclusion

Referring to the overall teleroperation scheme as in figure 1.2, this research focused on the slave side, precisely on the interaction of the robot with the physical surrounding. It embraced several existing theories and previous implementations, overarching them in order to move a step toward a spatial classification of the dynamic properties of the environment. Simulations first, and experimental tests later, have been used to demonstrate the validity of the treated theory. In particular, the results have been obtained using a realistic robotic arm, as envisioned within a real application, *de facto* laying the foundations to follow up with

further investigations while maintaining this principle. The main objective within i-Botics is to combine the cognitive ability of the human operator with the robotic capabilities at a distance, focusing on the “situational awareness” of the human operator and the robotic sensing/actuating capabilities. And the measure of fidelity of the VR with respect to the real world will determine the level of immersion and naturalness felt by the operator which, in turn, affects the fulfilment (or not) of certain delicate tasks. The outcome of this research poses answers, while suggesting further possible directions to take, so as to improve the current implementation, expand our knowledge and contribute to the cause of i-Botics. Although the last two decades have seen teleoperated robots becoming commonplace tools and necessity in many fields, the current technology is still far away from the utopian concept of *full telepresence*, as envisioned by many.

A Supplementary material

A.1 Additional plots

A.1.1 Simulations

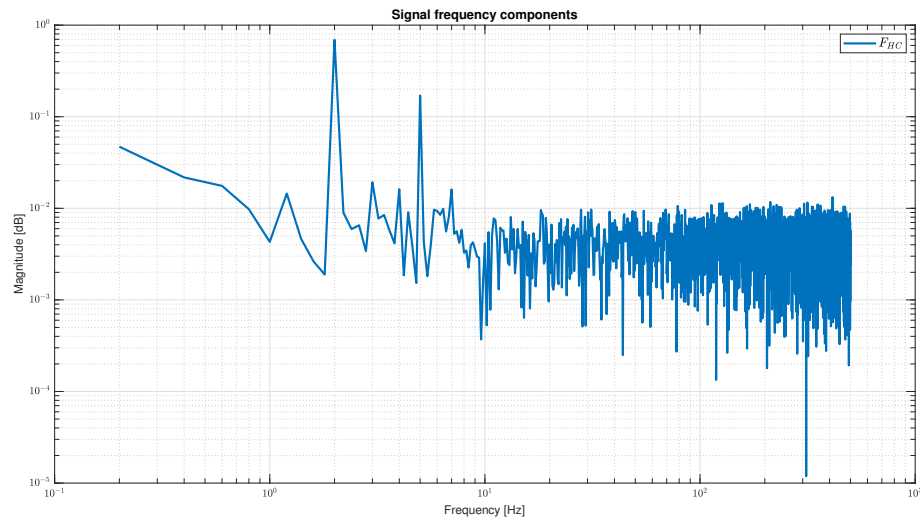


Figure A.1: Simulations: frequency content of the reference end-effector position ($T_s = 0.001$ s).

A.1.2 Elastic environment

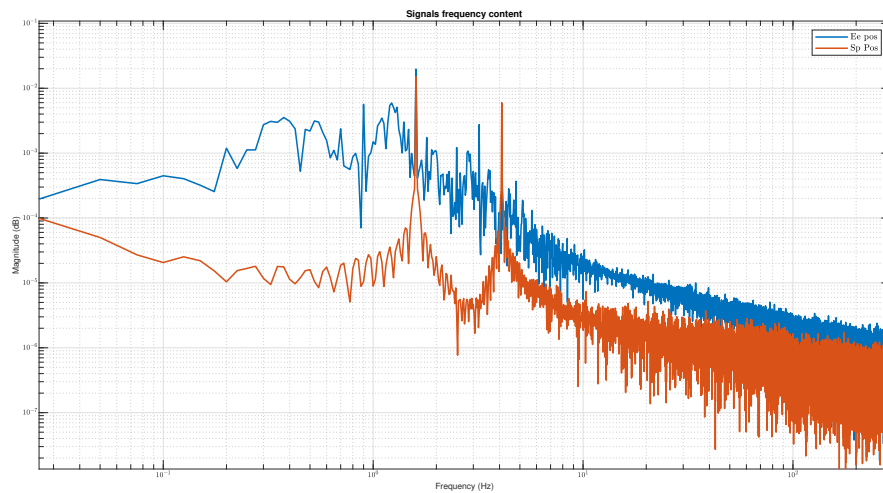


Figure A.2: Elastic environment: frequency content of the SP and measured position.

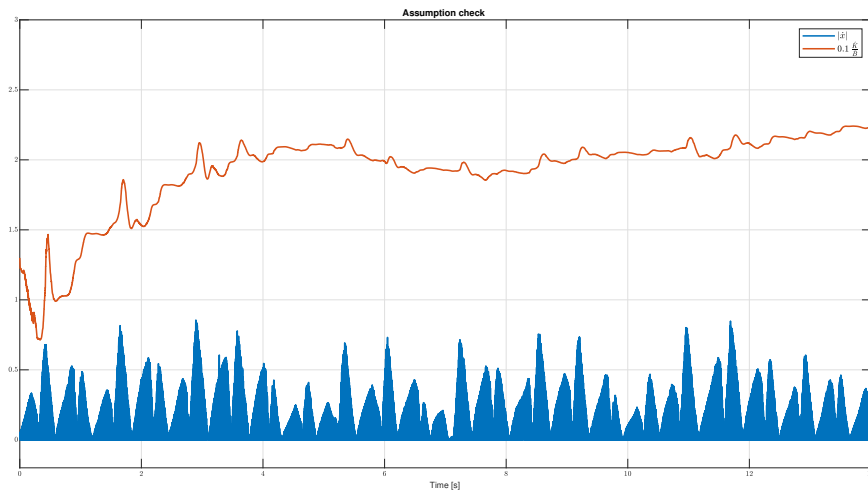


Figure A.3: Elastic environment: assumption check about linearization validity.

A.1.3 Spongy environment

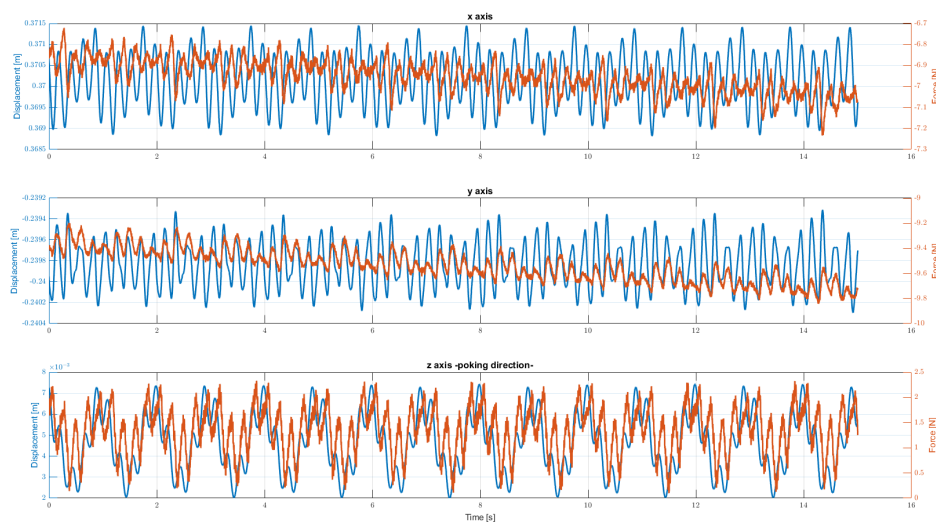


Figure A.4: Spongy environment: coupling effects and measured forces/positions.

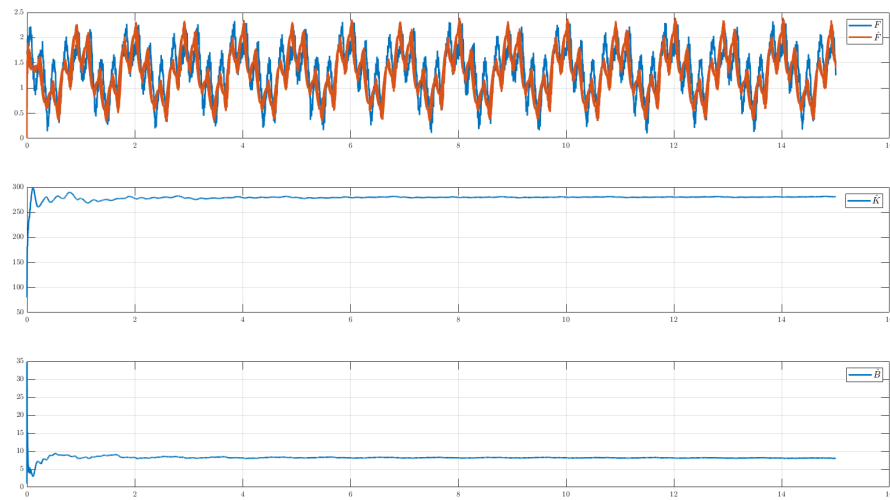


Figure A.5: Spongy environment: \hat{K} and \hat{B} .

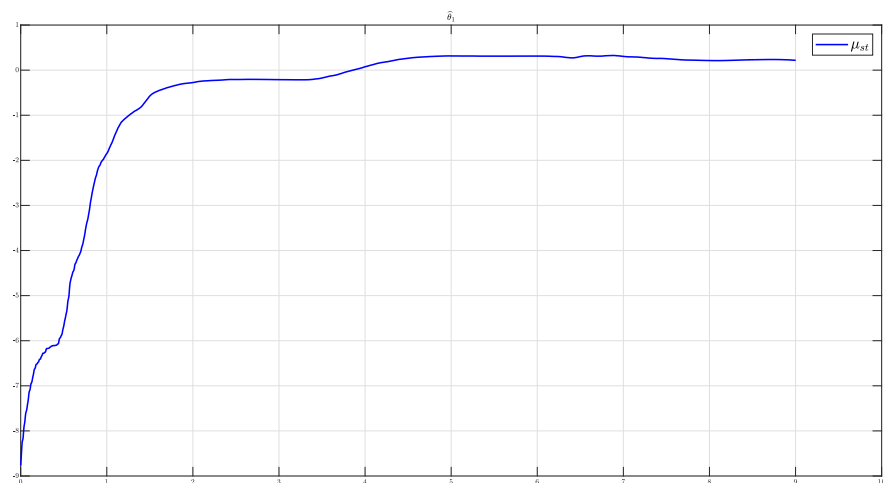


Figure A.6: Spongy environment: equivalent friction constant μ_{eq} .

A.1.4 Silicone environment: Ecoflex 50

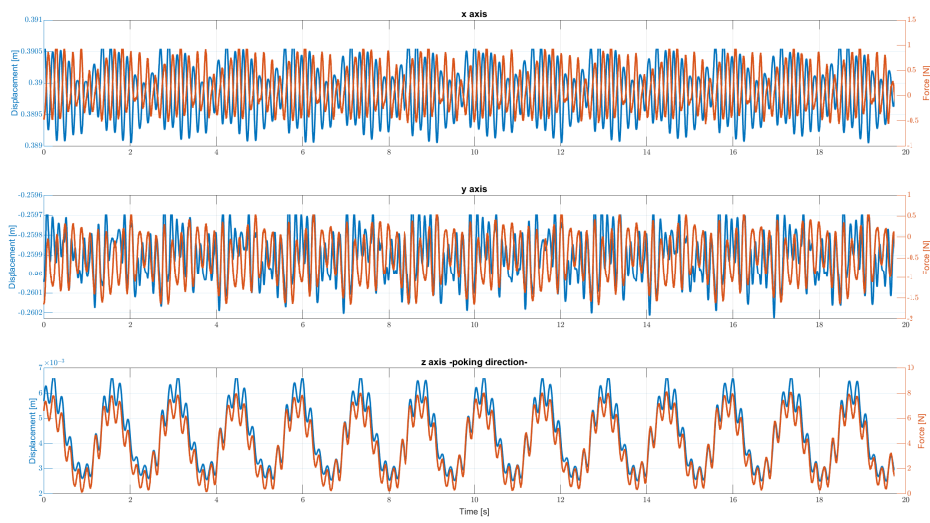


Figure A.7: Silicone Ecoflex 50: coupling effects and measured forces/positions.

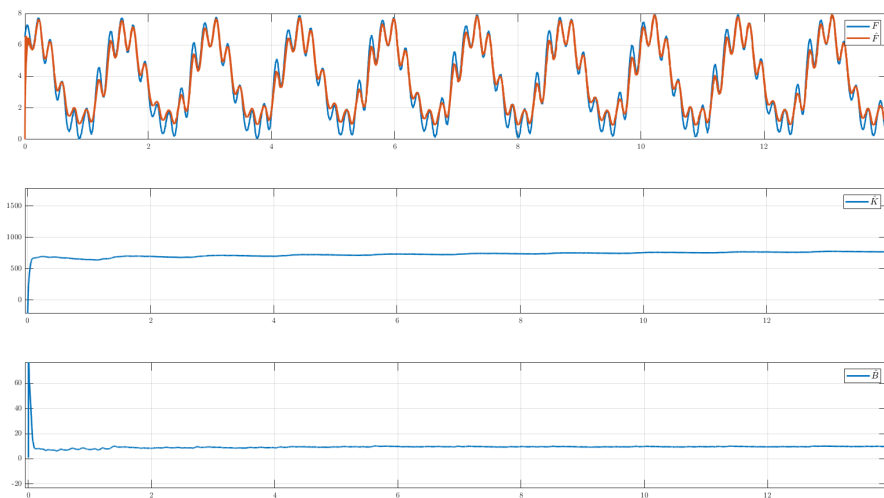


Figure A.8: Silicone Ecoflex 50: \hat{K} and \hat{B} .

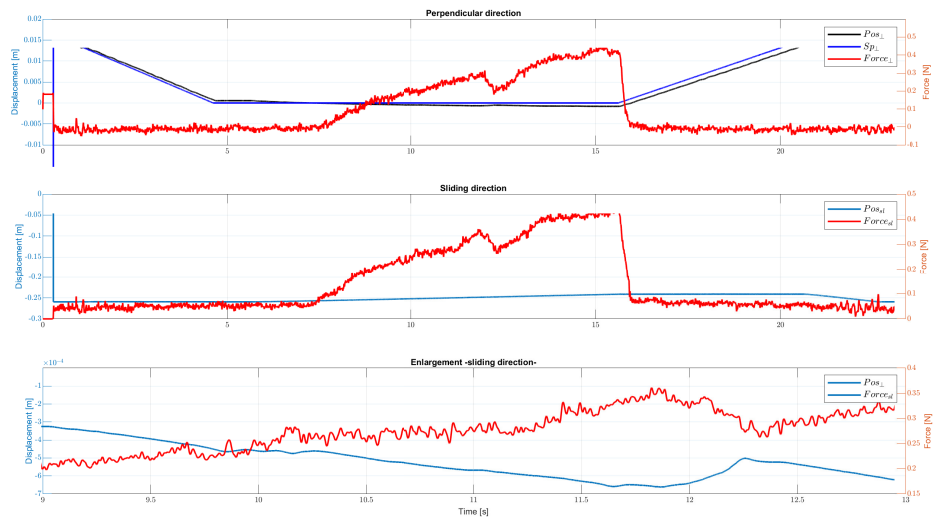


Figure A.9: Silicone Ecoflex 50: sliding.

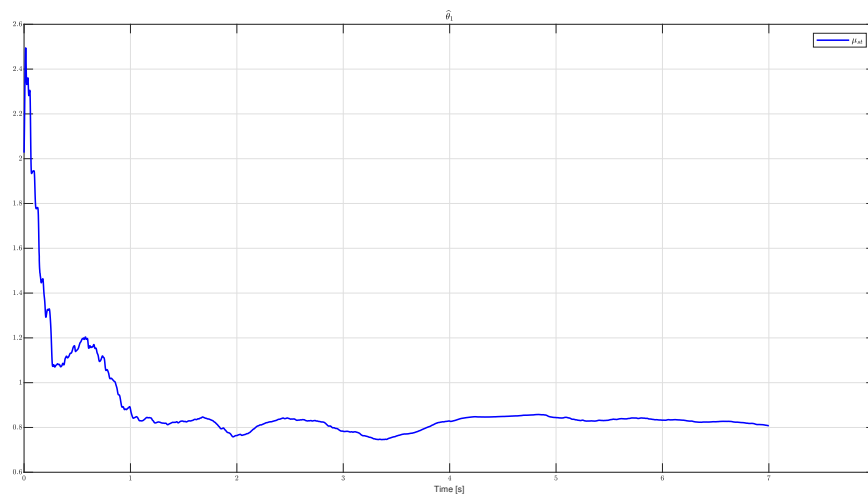


Figure A.10: Silicone Dragon skin 10: equivalent friction constant μ_{eq} .

A.1.5 Silicone environment: Dragon skin 10

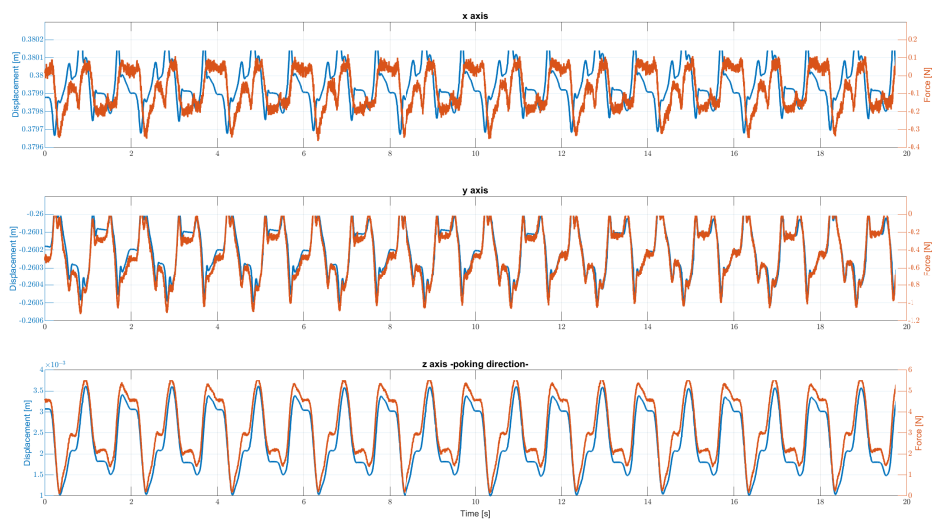


Figure A.11: Silicone Dragon skin 10: coupling effects and measured forces/positions.

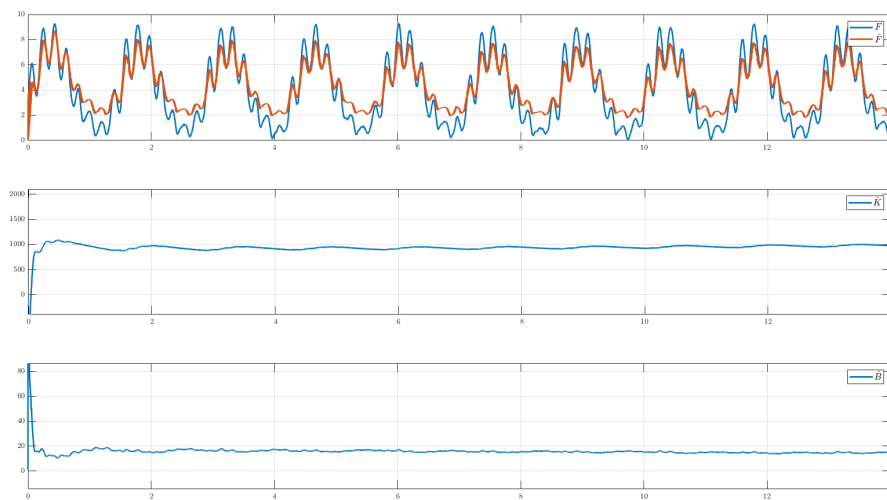


Figure A.12: Silicone Dragon skin 10: \hat{K} and \hat{B} .

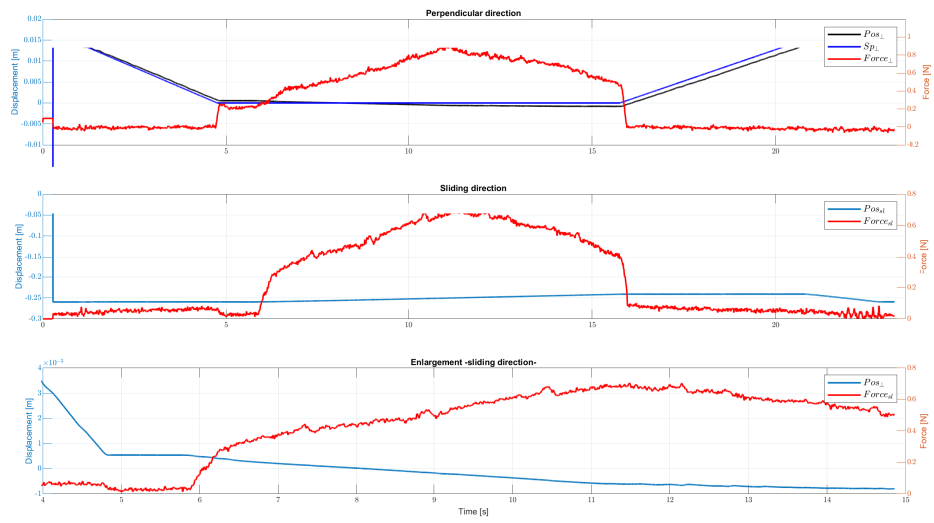


Figure A.13: Silicone Dragon skin 10: sliding.

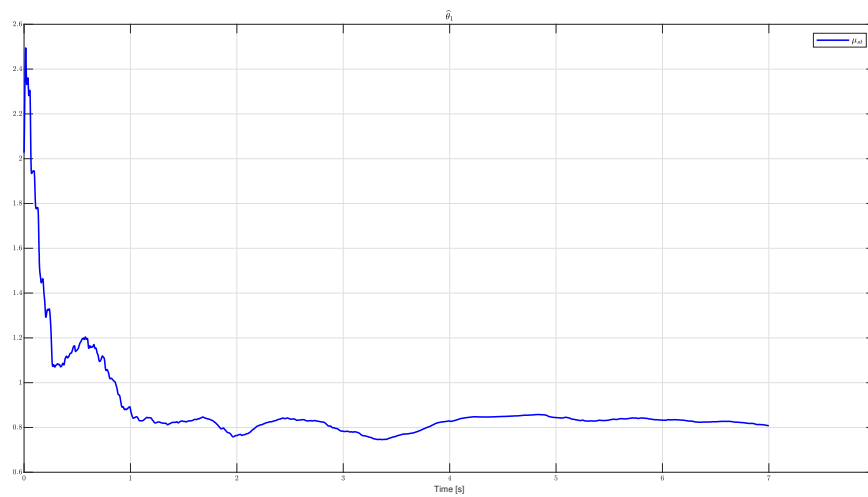


Figure A.14: Silicone Dragon skin 10: equivalent friction constant μ_{eq} .

A.1.6 Silicone environment: Dragon skin 10

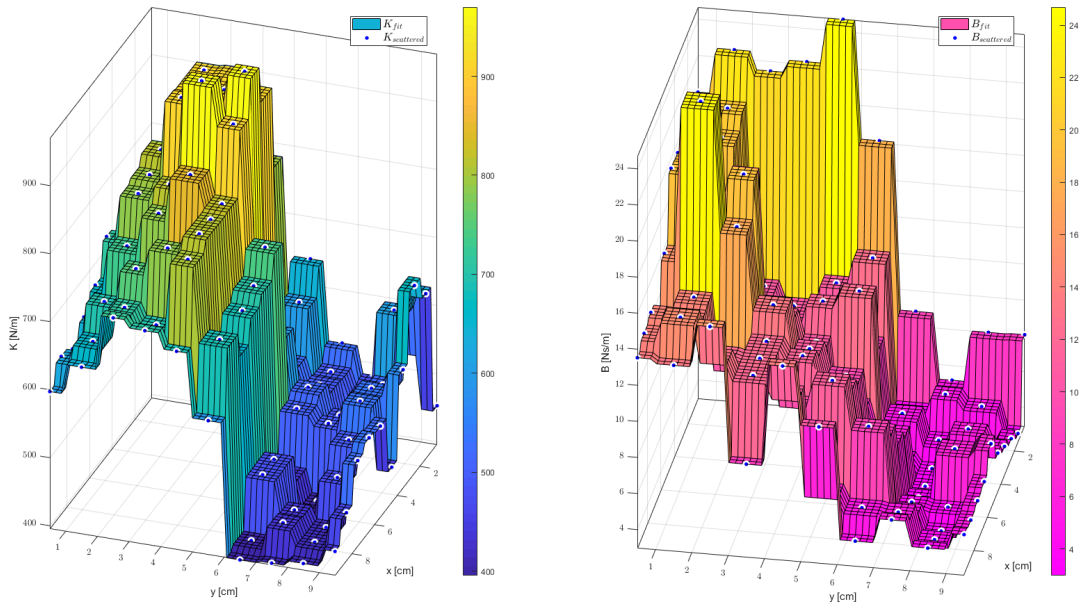
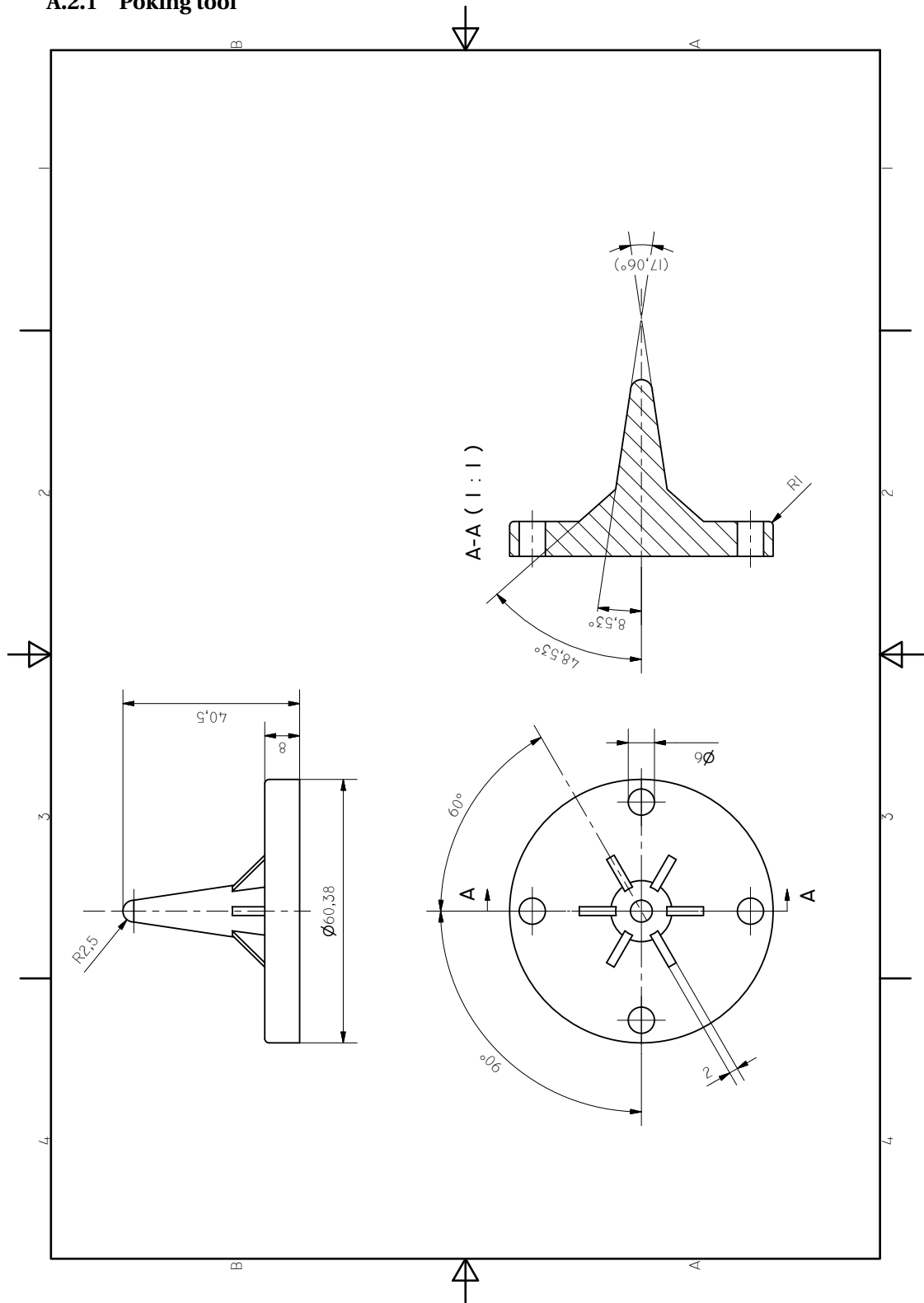


Figure A.15: Mixed environment: estimated stiffness $K(x, y)$. Nearest interpolation.

A.2 Drawings

A.2.1 Poking tool



Bibliography

- Abdossalami, A. and S. Sirouspour (2008), Adaptive control of haptic interaction with impedance and admittance type virtual environments, in *Haptic interfaces for virtual environment and teleoperator systems, 2008. haptics 2008. symposium on*, IEEE, pp. 145–152.
- Biagiotti, L. and C. Melchiorri (2007), Environment estimation in teleoperation systems, in *Advances in telerobotics*, Springer, pp. 211–231.
- Bicchi, A., J. K. Salisbury and D. L. Brock (1993), Experimental evaluation of friction characteristics with an articulated robotic hand, in *Experimental Robotics II*, Springer, pp. 153–167.
- Broenink, J. F. (1999), Introduction to physical systems modelling with bond graphs, *SiE Whitebook on Simulation Methodologies*, vol. 31.
- Colgate, J. E. and J. M. Brown (1994), Factors affecting the z-width of a haptic display, in *Robotics and Automation, 1994. Proceedings., 1994 IEEE International Conference on*, IEEE, pp. 3205–3210.
- Cortês, R., J. Park and O. Khatib (2006), Real-time adaptive control for haptic telemanipulation with kalman active observers, vol. 22, no.5, pp. 987–999.
- De Gerssem, G., H. Van Brussel and J. Vander Sloten (2005), Enhanced haptic sensitivity for soft tissues using teleoperation with shaped impedance reflection, in *Proceedings of the First Joint Eurohaptics Conference and Symposium on Haptic Interfaces for Virtual Environment and Teleoperator systems*.
- Diolaiti, N., C. Melchiorri and S. Stramigioli (2005), Contact impedance estimation for robotic systems, vol. 21, no.5, pp. 925–935.
- Dupont, P. E., C. T. M. Schulteis, P. A. Millman and R. D. Howe (1999), Automatic identification of environment haptic properties, vol. 8, no.4, pp. 394–411.
- Erickson, D., M. Weber and I. Sharf (2003), Contact stiffness and damping estimation for robotic systems, vol. 22, no.1, pp. 41–57.
- Franken, M., S. Stramigioli, S. Misra, C. Secchi and A. Macchelli (2011), Bilateral telemanipulation with time delays: A two-layer approach combining passivity and transparency, vol. 27, no.4, pp. 741–756.
- Franken, M., S. Stramigioli, R. Reilink, C. Secchi, A. Macchelli et al. (2009), Bridging the gap between passivity and transparency., in *Robotics: Science and Systems*.
- Franklin, G. F., J. D. Powell, A. Emami-Naeini and J. D. Powell (1994), *Feedback control of dynamic systems*, volume 3, Addison-Wesley Reading, MA.
- Fuentes-Pacheco, J., J. Ruiz-Ascencio and J. M. Rendón-Mancha (2015), Visual simultaneous localization and mapping: a survey, vol. 43, no.1, pp. 55–81.
- Gilardi, G. and I. Sharf (2002), Literature survey of contact dynamics modelling, vol. 37, no.10, pp. 1213–1239.

- Goertz, R. C. (1952), Fundamentals of general-purpose remote manipulators, *Nucleonics (US) Ceased publication*, **vol. 10**.
- Goertz, R. C. (1954), Mechanical master-slave manipulator, *Nucleonics (US) Ceased publication*, **vol. 12**.
- Haddadi, A. and K. Hashtrudi-Zaad (2008), A new method for online parameter estimation of hunt-crossley environment dynamic models, in *Intelligent Robots and Systems, 2008. IROS 2008. IEEE/RSJ International Conference on*, IEEE, pp. 981–986.
- Haddadi, A. and K. Hashtrudi-Zaad (2012), Real-time identification of Hunt–Crossley dynamic models of contact environments, **vol. 28**, no.3, pp. 555–566.
- Hannaford, B. (1989a), A design framework for teleoperators with kinesthetic feedback, **vol. 5**, no.4, pp. 426–434.
- Hannaford, B. (1989b), Stability and performance tradeoffs in bi-lateral telemanipulation, in *Robotics and Automation, 1989. Proceedings., 1989 IEEE International Conference on*, IEEE, pp. 1764–1767.
- Hannaford, B. and P. Fiorini (1988), Detailed model of bi-lateral teleoperation, in *Proceedings of the 1988 IEEE International Conference on Systems, Man, and Cybernetics*.
- Hashtrudi-Zaad, K. and S. E. Salcudean (1996), Adaptive transparent impedance reflecting teleoperation, in *Robotics and Automation, 1996. Proceedings., 1996 IEEE International Conference on*, volume 2, IEEE, pp. 1369–1374.
- Henry, P., M. Krainin, E. Herbst, X. Ren and D. Fox (2010), RGB-D mapping: Using depth cameras for dense 3D modeling of indoor environments, in *In the 12th International Symposium on Experimental Robotics (ISER, Citeseer*.
- Ho, C.-H., C. Basdogan and M. A. Srinivasan (1999), Efficient point-based rendering techniques for haptic display of virtual objects, **vol. 8**, no.5, pp. 477–491.
- Hoeba, N., N. van der Stap and D. Abbink (2018), Report: Internship TNO, TNO, i-Botics.
- Hogan, N. (1985), Impedance control: An approach to manipulation: Part II—Implementation, **vol. 107**, no.1, pp. 8–16.
- Hokayem, P. F. and M. W. Spong (2006), Bilateral teleoperation: An historical survey, **vol. 42**, no.12, pp. 2035–2057.
- Hunt, K. and F. Crossley (1975), Coefficient of restitution interpreted as damping in vibroimpact, **vol. 42**, no.2, pp. 440–445.
- Jeon, S. and S. Choi (2009), Haptic augmented reality: Taxonomy and an example of stiffness modulation, **vol. 18**, no.5, pp. 387–408.
- Jeon, S. and S. Choi (2010), Stiffness modulation for haptic augmented reality: Extension to 3D interaction, in *Haptics Symposium, 2010 IEEE*, IEEE, pp. 273–280.
- Klatzky, R. L., S. J. Lederman and V. A. Metzger (1985), Identifying objects by touch: An “expert system”, **vol. 37**, no.4, pp. 299–302.
- Lawrence, D. A. (1992), Designing teleoperator architectures for transparency, in *Robotics and Automation, 1992. Proceedings., 1992 IEEE International Conference on*, IEEE, pp. 1406–1411.

- Lederman, S. J. and R. L. Klatzky (1987), Hand movements: A window into haptic object recognition, **vol. 19**, no.3, pp. 342–368.
- Lederman, S. J. and R. L. Klatzky (1990), Haptic classification of common objects: Knowledge-driven exploration, **vol. 22**, no.4, pp. 421–459.
- Ljung, L. (1998), System identification, in *Signal analysis and prediction*, Springer, pp. 163–173.
- Love, L. J. and W. J. Book (1995), Environment estimation for enhanced impedance control, in *Robotics and Automation, 1995. Proceedings., 1995 IEEE International Conference on*, volume 2, IEEE, pp. 1854–1859.
- Love, L. J. and W. J. Book (2004), Force reflecting teleoperation with adaptive impedance control, **vol. 34**, no.1, pp. 159–165.
- Marhefka, D. W. and D. E. Orin (1999), A compliant contact model with nonlinear damping for simulation of robotic systems, **vol. 29**, no.6, pp. 566–572.
- Misra, S. and A. M. Okamura (2006), Environment parameter estimation during bilateral telemanipulation, in *Haptic Interfaces for Virtual Environment and Teleoperator Systems, 2006 14th Symposium on*, IEEE, pp. 301–307.
- Murthy, S. T. (2010), *Textbook of Elements of Mechanical Engineering, Revised Third Edition*, International Publishing House.
- Na, U. J. and M. H. Vu (2012), Adaptive impedance control of a haptic teleoperation system for improved transparency, in *Haptic Audio Visual Environments and Games (HAVE), 2012 IEEE International Workshop on*, IEEE, pp. 38–43.
- Narendra, K. S. and A. M. Annaswamy (2012), *Stable adaptive systems*, Courier Corporation.
- Nijof, S. (2018), Teleoperation using passive control and LUNA network channels, RaM, uTwente.
- Nüchter, A., K. Lingemann, J. Hertzberg and H. Surmann (2007), 6D SLAM—3D mapping outdoor environments, **vol. 24**, no.8-9, pp. 699–722.
- Ogata, K. (2002), *Modern control engineering*, volume 4, Prentice hall India.
- Ott, C., R. Mukherjee and Y. Nakamura (2010), Unified impedance and admittance control, in *Robotics and Automation (ICRA), 2010 IEEE International Conference on*, IEEE, pp. 554–561.
- Salisbury, K., F. Conti and F. Barbagli (2004), Haptic rendering: introductory concepts, **vol. 24**, no.2, pp. 24–32.
- Schmidt, R. M., G. Schitter and A. Rankers (2014), *The Design of High Performance Mechatronics: High-Tech Functionality by Multidisciplinary System Integration*, IOS Press.
- Seraji, H., D. Lim and R. Steele (1996), Experiments in contact control, **vol. 13**, no.2, pp. 53–73.
- Sheridan, T. B. (1989), Telerobotics, **vol. 25**, no.4, pp. 487–507.
- Sheridan, T. B. (1993), Space teleoperation through time delay: Review and prognosis, **vol. 9**, no.5, pp. 592–606.

- Shimoga, K. B. (1993), A survey of perceptual feedback issues in dexterous telemanipulation. II. Finger touch feedback, in *Virtual Reality Annual International Symposium, 1993.*, 1993 *IEEE*, IEEE, pp. 271–279.
- Siciliano, B. and O. Khatib (2016), *Springer handbook of robotics*, Springer.
- Slotine, J.-J. E. and W. Li (1989), Composite adaptive control of robot manipulators, **vol. 25**, no.4, pp. 509–519.
- Stramigioli, S. (1998), *From differentiable manifold to interactive robot control*, Ph.D. thesis, TU Delft, Delft University of Technology.
- Tzafestas, C., S. Velanas and G. Fakiridis (2008), Adaptive impedance control in haptic teleoperation to improve transparency under time-delay, in *Robotics and Automation, 2008. ICRA 2008. IEEE International Conference on*, IEEE, pp. 212–219.
- Ueberle, M., H. Esen, A. Peer, U. Unterhinninghofen and M. Buss (2009), Haptic feedback systems for virtual reality and telepresence applications, *Feedback*, **vol. 56**, p. 97.
- Van Geffen, V. (2009), A study of friction models and friction compensation, *DCT*, **vol. 118**, p. 24.
- Velanas, S. V. and C. S. Tzafestas (2010), Human telehaptic perception of stiffness using an adaptive impedance reflection bilateral teleoperation control scheme, in *RO-MAN, 2010 IEEE*, IEEE, pp. 21–26.
- Yamamoto, T., M. Bernhardt, A. Peer, M. Buss and A. M. Okamura (2008), Techniques for environment parameter estimation during telemanipulation, in *Biomedical Robotics and Biomechatronics, 2008. BioRob 2008. 2nd IEEE RAS & EMBS International Conference on*, IEEE, pp. 217–223.